Liu Bing (Orcid ID: 0000-0002-7790-9218)

Chang Xuexiang (Orcid ID: 0000-0001-5145-2283)

Hydrochemical characteristics jointly determine the transport and cycling of soil carbon, nitrogen, and phosphorus in an arid Chinese wetland

Bing LIU[1,*], [1]Wenzhi ZHAO[1], Zijuan WEN[2], Yuting YANG[3], Xuexiang CHANG[1], Zhaocen ZHU[1], Rui SI[1]

1. Linze Inland River Basin Research Station, Key Laboratory of Ecohydrology of Inland River Basin, Northwest Institute of Eco-Environment and Resources, Chinese Academy of Sciences, Lanzhou 730000, China. 2. *School of Mathematics and Statistics, Lanzhou University, Lanzhou 730000, China.* 3. *State Key Laboratory of Hydroscience and Engineering, Department of Hydraulic Engineering, Tsinghua University, Beijing 10084, China*

* Corresponding author. Tel.: +86 931 4967139.

E-mail: liubing@lzb.ac.cn

Received: Accepted:

This article has been accepted for publication and undergone full peer review but has not been through the copyediting, typesetting, pagination and proofreading process which may lead to differences between this version and the Version of Record. Please cite this article as doi: 10.1029/2020JG005697

Key Points:

We simulated the variations of hydrochemical characteristics and the storage and stoichiometry of C, N, and P

The model that coupled the Hydrus-1D and DNDC model to solve a drawback of hydrochemical simulation

We identified the mechanisms by which hydrochemical characteristics determine the transport and cycling of soil nutrient

Abstract

Salt accumulation gradually changes the cycling of carbon (C), nitrogen (N), and phosphorus (P), and may even transform sinks into sources in arid wetlands. However, it's not clear how hydrochemical characteristics affect the wetland's source or sink function, or how they affect C, N, and P cycling in arid regions. To clarify these relationships, we conducted field measurement in arid northern China. We simulated the variations of hydrochemical characteristics and the storage and stoichiometry of C, N, and P using the process-based DNDC and Hydrus-1D models. The meteorological and hydrological processes had obvious characteristics of seasonal and interannual changes. The measured evapotranspiration averaged 660.23 and 587.94 mm yr^{-1} in the saltmarsh and riparian wetlands, respectively. The soil showed a clear trend with a higher of SO_4^{2-}, Na^+, Ca^{2+}, and Cl^- fractions in comparison with a lower of Mg^{2+}, K+, and HCO_3^- fractions, with the major ion and nutrient concentrations gradually decreasing with increasing depth in the soil. The major ion types had characteristics of Na^+-Ca^{2+}-SO_4^{2-}-Cl^- in the saltmarsh wetland and riparian wetland. The storage of total C, N, and P were 372.72±66.52 t C/hm^2,10.92±2.59 t N/hm^2, and 17.55±1.54 t P/hm^2in the saltmarsh wetland, versus 119.72±27.88 t C/hm^2, 4.38±1.24 t N/hm^2, and 13.17±1.46 t P/hm^2 in the riparian wetland. Therefore, wetland salinization in our study led to increased soil C, N, and P contents and storage, and thereby enhanced the sink function of the wetlands.

Keywords: hydrochemical characteristics; ion concentrations; nutrient concentrations; carbon; nitrogen; phosphorus.

1. Introduction

Wetlands are important organic carbon reservoirs in arid regions, where they play an important role in maintaining CO_2 sinks, CH_4 sources, and ecological balances (Li et al., 2005; Castañeda and Herrero, 2008). Over the past century, changes in the hydrological regime and salt concentration of wetlands caused by global climate change and human activities have led to significant degradation and salinization of arid wetlands (Nielsen et al., 2003,Li et al. 2006; Jolly et al., 2008; Huckelbridge et al., 2010; Li and Zhao, 2010; Gran et al., 2011), and these changes seriously threaten the stability of oases and the health of wetland ecosystems. Simultaneously, salt accumulation changes soil physical and chemical properties. The stress created by salt ions can decrease plant primary productivity and organic matter accumulation, thereby changing microbial mineralization of organic matter and the cycling of key nutrient elements such as carbon (C), nitrogen (N) and phosphorus (P) (Neubauer, 2013). These changes, in turn, affect the storage and emission of C and N, and may even cause the transformation of sinks into sources (or vice versa) in arid wetlands (Chambers et al., 2013; Neubauer, 2013). Therefore, we begin to suspect whether saline wetlands can continue to maintain their function as a C sink under the pressures created by these changes. In addition, the alternation between periodic exposure and submergence of groundwater in transient wetlands creates active migration and transformation of C, N, and P in arid wetlands. As a result, the accumulation of C, N, and P vary greatly both spatially and temporally and have a unique distribution in arid wetlands (Cheng et al., 2010; Zhang et al., 2013). However, the mechanisms for how the hydrochemical characteristics affect the balance, source/sink function, and cycles of C, N, and P in arid regions are not yet clearly understood (Winter, 2000; Johnson et al., 2005; Couto et al., 2013; Drexler et al., 2013; Morrissey et al., 2014; Weston et al., 2014; Finger et al., 2016; Zou et al., 2018; Wang et al., 2019).

Wetlands can change between being a source and being a sink, and the hydrological conditions and chemical characteristics affect the source/sink status through changes in soil C, N, and P storage and migration processes (Tavakkoli et al., 2011; Feng et al., 2014). These changes can lead to high spatial and temporal heterogeneity in the distribution of biogeochemical processes in arid wetlands (Couto et al., 2013; Drexler et al., 2013; Weston et al., 2014). In arid wetlands, precipitation is rare, so the effluence of shallow groundwater,

agricultural irrigation, and river water are the main water sources (Liu et al., 2014, 2017). Seasonal and interannual variability in precipitation and groundwater depth affects the freshwater (river) discharge into wetlands and influences the transport of watershed-derived nutrients and sediments (Pont et al., 2002; Neubauer, 2013). This alters solute transport, hydrochemical characteristics, and organic matter accumulation and decomposition processes, so that soil C and N stocks often decrease from drawdown of the water table depth caused by increased frequency and intensity of climate extremes and increasing human activities in and around wetlands (Weston et al., 2010; van Dijk et al., 2015).

Simultaneously, soil moisture influences C sequestration and release, decomposition of litter and soil organic matter, and root turnover and respiration by changing the litter properties, soil redox conditions, and microbial activity (Lamers et al., 2013; Van Diggelen et al., 2015). Therefore, changes in the water conditions can have positive and negative effects on soil C mineralization and C sequestration or emission in wetlands, leading to high uncertainty about the effects on soil C stocks. In addition, soil salinization increases ionic concentrations that regulate soil permeability, temperature, redox potential, and microbial activity in arid wetlands (Sperling et al., 2014; Sutter et al., 2014). This can influence the conversion and accumulation processes for soil C, N, and P (Chambers et al., 2011; van Dijk et al., 2015; Weston et al., 2014; Vizza et al., 2017), including nitrification (Noe et al., 2013), denitrification (Marks et al., 2016), and P availability, and promote the transformation of the ecosystem into a C source or sink (Tong et al., 2010; Xu et al., 2014). Although researchers have made considerable progress in understanding soil C and N cycles in natural wetlands around the world (Page and Dalal, 2011; Juszczak and Augustin, 2013; Song et al., 2009; Tong et al., 2013), there have been few studies of soil C, N, and P storage and migration in arid wetlands. Nonetheless, the hydrochemical characteristics of arid wetlands determine the transport and cycling of C, N, and P, so it's necessary to study the effects of the hydrological conditions and chemical characteristics on these cycles to provide a scientific basis and theoretical reference for reducing CO_2 and CH_4 emission in arid wetlands.

Saline wetlands in arid regions are a highly sensitive part of the global carbon cycle (Wang et al., 2019). Increasing carbon sequestration by wetland soils appears to be an immediately viable option to increase the global soil carbon pool, thereby reducing levels of atmospheric CO_2 and mitigating global warming (Sun et al., 2013). Restoration of these carbon stocks requires an improved ability to predict how hydrological feedbacks affect ecological processes. Thus, researchers are increasingly simulating the changes of soil C, N, and P over broad spatial and temporal scales by using process-based models (Giltrap et al., 2010; Xu et al., 2014). For example, the DNDC (DeNitrification-DeComposition) model has been widely applied to simulate the biogeochemical cycles of C and N by simulating the main processes of denitrification and decomposition that occur in agricultural systems (Li et al., 1992, 2012; Giltrap et al., 2010; Deng et al., 2011). DNDC contains six interacting sub-models: soil, climate, crop vegetation, decomposition, denitrification, and nitrification (Li et al., 2017a). The original version of DNDC has been modified to derive various site-specific and regional versions by adjusting the model's parameters and equations to more accurately simulate overall C and N biogeochemical cycles. For example, it has been used to scale up estimates of soil organic matter generation, decomposition, and transformation from the plot level to a regional scale (Li et al., 2017b), and to predict the contents of soil organic carbon components and greenhouse gases such as CO_2, N_2O, CH_4, and NO (Deng et al., 2011; Cui and Wang, 2019). This method has been validated internationally through long-term applications at a plot scale, with studies in grassland, wetland, woodland, and other terrestrial ecosystems in North America, Europe, and Asia (Pathak et al., 2005; Li et al., 2015a, b). It is now one of the most widely accepted biogeochemical models in the world (Tang et al., 2006; Li et al., 2017a, b). However, there have been no simulations of the transport and cycling of C, N, and P using process-based models for China's arid wetlands.

To improve our understanding of these cycles in arid wetlands, we conducted field measurements of two types of wetland in arid northern China. Based on this data, we used DNDC and the Hydrus-1D model to simulate seasonal and interannual variations of

hydrochemical processes in these ecosystems, and their effects on C, N, and P cycling. Our specific objectives were (1) to calibrate the model parameters using field measurements of the hydrochemical parameters; (2) to simulate seasonal and interannual variations of major ion and nutrient concentrations; (3) to evaluate how these hydrochemical characteristics affect C, N, and P cycling; and (4) to ascertain how the hydrochemical characteristics affect nutrient balances, source/sink functions, and cycles of C, N and P. We present the results of these measurements and model simulations to illustrate how hydrochemical characteristics influence the storage of total C, N, and P in arid wetlands.

2. Methodology

2.1. Model Development

2.1.1. Water transport

One-dimensional water movement in homogeneous, rigid porous media with variable saturation is described by the Richards equation (Šimůneket al., 2013):

$$\frac{\partial \theta}{\partial t} = \frac{\partial}{\partial z}[K(h)(\frac{\partial h}{\partial z} - 1)] - s(z,t) \quad (1)$$

where θ is the volumetric water content (cm^3cm^{-3}), t is time, z is the vertical coordinate (positive values are downward from the soil surface), h is the hydraulic (pressure) head (cm), $K(h)$ is the hydraulic conductivity (cmd^{-1}) as a function of the hydraulic head, and s is the root water uptake rate ($cm^3\ cm^{-3}\ d^{-1}$), which follows the Feddes et al. (1978) function.

van Genuchten (1980) used the statistical pore-size distribution to obtain a predictive equation for the unsaturated hydraulic conductivity function in terms of soil water retention parameters:

$$\theta = \begin{cases} \theta_r + \dfrac{\theta_s - \theta_r}{[1 + |ah|^n]^m} & h < 0 \\ \theta_s & h \geq 0 \end{cases} \quad (2)$$

$$K(h) = K_s S_e^l [1-(1-S_e^{1/m})^m]^2 \quad h<0 \qquad (3)$$

$$S_e = \frac{\theta - \theta_r}{\theta_s - \theta_r} \quad (4)$$

where θ_r and θ_s are the residual and saturated water contents, respectively, which can be determined from experimental data; K_s is the saturated hydraulic conductivity; α is the inverse of the air-entry value (or bubbling pressure), n is a pore-size distribution index, m = 1–(1/n); and S_e is the effective saturation. The parameters α, n, and l are empirical coefficients that affect the shape of the hydraulic functions.

2.1.2 Solute transport

We used the following partial differential equation to describe the one-dimensional, convective–dispersive mass transport under transient water flow conditions in a partially saturated porous medium:

$$\frac{\partial \theta c}{\partial t} = \frac{\partial \theta}{\partial z}(\theta D \frac{\partial \theta}{\partial z}) - \frac{\partial qc}{\partial z} \quad (5)$$

where c is the major ion concentrations for dominant hydrochemicals (SO_4^{2-}, Cl^-, HCO_3^-, Ca^{2+}, Mg^{2+}, K^+, Na^+) (ML^{-3}). D is the effective dispersion coefficient ($L^2\ T^{-1}$), and q is the volumetric flux density given by Darcy's law ($L^3\ L^{-2}\ T^{-1}$). D is calculated using the following equation:

$$D = aLq \quad (6)$$

where L represents the longitudinal dispersivity (L). Eq. (6) assumes that molecular diffusion is insignificant relative to dispersion.

2.2. Boundary conditions

We used depth to groundwater measurements to describe the bottom boundary of the soil profile, and assumed free drainage at the bottom boundary. There was no noticeable surface

runoff during the study period, and the top boundary conditions were defined by evapotranspiration and precipitation. We assumed that there was no heat storage, and integrated the energy balance for the boundary conditions for the heat and water transport equations. Under these conditions, the energy exchange in the infinitesimal air layer just above the soil surface can be expressed by the following surface energy balance equation (Saito et al., 2006):

$$R_n - G - H - \lambda ET = 0 \quad (7)$$

where R_n is the net radiation flux ($W \cdot m^{-2}$), G is the soil heat flux ($W \cdot m^{-2}$), λ is the latent heat of evaporation (2.45 $MJ \cdot kg^{-1}$), and ET represents evapotranspiration (mm). The Bowen ratio ($\beta = \gamma \triangle T / \triangle e_a$), where ΔT represents the temperature ($°C^{-1}$) difference, and Δe_a represents the corresponding vapor-pressure difference between 1 and 2 m above the crop canopy, can be expressed as the ratio of the sensible heat flux (R_n–G) to the latent heat flux ($H/\lambda ET$), and the actual evapotranspiration can be calculated as follows:

$$ET = \frac{1}{\lambda}\left(\frac{R_n - G}{(1 + \gamma \Delta T / \Delta e_a)}\right) \quad (8)$$

where γ is the psychrometric constant ($kPa \cdot °C^{-1}$).

2.3. Model integration and solution

The Hydrus-1D model numerically solves the Richards equation to simulate water and solute transport in one-dimensional unsaturated, partially saturated, or fully saturated porous media (Šimůnek et al., 2013). Simultaneously, the DNDC model can simulate biogeochemical cycles for C, N, and P at a point scale and at a regional scale (Yu et al., 2018; Zou et al., 2018;Cui and Wang, 2019). This can solve a drawback of the Hydrus program, which cannot easily simulate C, N, and P cycles. We used version 9.5 of DNDC (http://www.dndc.sr.unh.edu/) in this study, which is referred to as the original DNDC model. We fully coupled the models by replacing some modules in the Hydrus-1D mode with the DNDC model to simulate the dynamic processes for soil organic matter (SOM), total nitrogen

(TN), total carbon (TC), total phosphorus (TP), available nitrogen (AN), available phosphorus (AP), and available potassium (AK) and to solve the numerical model that coupled the water, solute, and nutrient transport mechanisms. This allowed the Hydrus-1D model to simulate groundwater, *ET*, and the transport of the major ions (SO_4^{2-}, Cl^-, HCO_3^-, Ca^{2+}, Mg^{2+}, K^+, Na^+). In this study, the water holding function was introduced to extract the hydraulic characteristics of soil, and the function was coupled to the soil hydrological model (Hydrus-1D) and Denitrification-Decomposition model (DNDC model). In addition, the coupling model replaced the soil hydrology module in the DNDC model with the Hydrus-1D model to describe the soil water flux more accurately. Water transport of structured porous media in the DNDC model were described using the dual-porosity functions and soil hydraulic properties in Hydrus-1D model.

The Hydrus-1D model simulated water flow equations 1 to 4 and solute concentration equations 5 and 6. We calibrated the Hydrus-1D model based on the volumetric soil water content (θ) and the soilsalinity, which we measured in the soil profiles in the saltmarsh wetland and riparian marsh. The simulation period was from 2014 to 2017. Two key soil hydraulic properties, the residual and saturated water contents (θ_r and θ_s), were measured in the laboratory from soil samples that were extracted from the field plots. The saturated hydraulic conductivity (K_s) was evaluated in the field using the method described in section 3.2.1. The parameters α, n, and l were optimized using the Levenberg–Marquardt method that was incorporated in the HYDRUS-1D code. The hydraulic parameters were measured in the field for both wetlands (Table 1).

[Table 1. near here]

The DNDC model simulated the dynamic processes in soil nutrient cycles based on the Langmuir equation. First, we input the parameters required by the DNDC model, which included daily climate data, soil parameters (density, texture, bulk density, porosity, humidity, temperature, pH, electrical conductivity, and concentrations of SOM, TN, TC, TP, AN, AP, and AK), and hydrological parameters (the depth to groundwater). We then compared the

simulation results with the data measured in the field, and calculated the accuracy of the simulation values using the error terms defined in section 3.3. We adjusted the parameters to improve the model's fit, and defined the parameters after this calibration as the model parameters.

3. Study sites and data collection

3.1. Study area

The study area (Fig. 1) is located in the national nature reserve in the Heihe River wetland, which is in the middle reaches of northwestern China's Heihe River basin (39°22'N–39°23'N, 100°07'E–100°08'E).The region is dominated by a continental arid temperate climate. The annual temperature averages 8.0°C, and the mean monthly temperature ranges from –15.5°C in January to 29.1°C in July. The mean annual frost-free period averages 153 days. The annual precipitation averages 125.3 mm, with about 65% of the total precipitation occurring with low intensity between July and September. Only 3% of the rain occurs during the winter. Potential *ET* averages 2047 mm. The soil is typically characterized as a gray desert soil or a desert soil. The wetlands are seasonal and temporary, and are mainly distributed in the Heihe River's riparian zone, in oases, in the spring overflow zone along the river bank, and in inland lakes and other seasonal or perennial bodies of water.

[Fig. 1. near here]

In the study area, riparian wetland and saltmarsh wetland are the main typical wetland types. We focused on a riparian wetland along the river and a saltmarsh wetland in the oasis zone, where there are no surface water inflows or outflows. Instead, these wetlands are supported by subsurface flows from the river, shallow groundwater, and leakage from farmland irrigation. The saltmarsh wetland is primarily wet meadows dominated by shrubs (*Tamarix chinensis*) and halophytic herbs (*Phragmites australis*, *Agropyron cristatum*, *Oxytropis glabra*, *Equisetum ramosissimum*, *Typha orientalis*, *Carex tangiana*). In the riparian zone, vegetation is distributed on or near the banks of the Heihe River and is

dominated by trees (*Populus alba*, *Elaeagnus angustifolia*, *Salix babylonica*), shrubs (*T. chinensis*), and herbs (*Carex karoi*, *Juncus articulatus*, *P. australis*, *Leymus secalinus*, *Sophora alopecuroides*).

3.2 Measurements

3.2.1 Soil moisture, salinity, and groundwater measurements

The experiments were conducted in the two wetlands from 2014 to 2017. We measured the volumetric soil water content and the electrical conductivity (*EC*, dSm^{-1}) using ECH_2O-10 dielectric probes (Decagon Devices, Pullman, WA, USA) buried at five depths below the soil surface (20, 40, 60, 80, and 100 cm), with three replications. We collected soil samples at eight depths (10, 20, 30, 40, 50, 60, 80, and 100) every 10 days to measure the soil water content and soil salinity in the laboratory, and to validate the soil moisture and *EC*. We performed regression analyses using *EC* as the independent variable and soil salinity (S_s, g kg^{-1}) as the dependent variable based on data in all depths' average (20, 40, 60, 80, and 100 cm), and developed empirical models for this relationship:

$S_s = 17.64\ln(EC)+8.12$, $R^2 = 0.94$, $n = 435$ for the saltmarsh wetland

$S_s = 5.96\ln(EC)+10.30$, $R^2 = 0.84$, $n = 525$ for the riparian wetland

Simultaneously, we automatically measured the depth to the water table and water temperature using a water-level sensor (HOBO water level logger, Onset Computer Corporation, Pocasset, MA, USA), and recorded the data every hour. Each of the five observation wells was 5 cm in diameter and made from PVC pipe; all wells had sensors installed. In addition, we measured soil bulk density, particle basic density, soil water content at the wilting point, and field capacity, and developed a water-retention curve and calculated the hydraulic conductivity. The soil parameters are shown in Table 2.

[Table 2. near here]

3.2.2Meteorological measurements

We used the Bowen ratio–energy balance method to measure *ET* and the water and energy fluxes at the interface between soil and the atmosphere in both wetlands. The data was collected using a micrometeorological system (Radiation Energy Balance Systems Inc., Bellevue, WA, USA) with sensors installed at 2 and 3 m above the ground. We measured air temperature and relative humidity using a temperature /humidity probe (MP300, Campbell Scientific Ltd., Shepshed, UK), wind speed and direction using a three-dimensional sonic anemometer (ATI Electronics Inc., Boulder, CO, USA), and atmospheric pressure and water vapor using an infrared gas analyzer (CS105, Vaisala, Helsinki, Finland). We observed R_n and the photosynthetically active photon flux density at a height of 2 m above the ground using a quantum sensor (LI190SB, Li-Cor Inc., Lincoln, NE, USA) and a four-component net radiometer (CNR-1, Kipp and Zonen, Delft, the Netherlands), and determined the soil heat flux using three soil heat-flux plates (model HFT-3, Radiation and Energy Balance Systems, Seattle, WA, USA) buried 5 m from the micrometeorological tower at a depth of 3 cm. We measured precipitation with a tipping-bucket rain gauge (model TE525, metric; Texas Electronics, Dallas, TX, USA), and monitored soil moisture (Decagon Devices) and soil temperature (107-L, Campbell Scientific Ltd., Edmonton, Alberta, Canada) adjacent to the micrometeorological tower at depths of 10, 20, 30, 40, 50, 60, 80, and 100 cm. We measured the meteorological data at a frequency of 10 Hz and recorded the data every 5 min using a CR1000 datalogger (Campbell Scientific Inc., Logan, UT, USA), which was stored as the 30-min mean. Precipitation and wind data were stored as the 10-min mean.

3.2.3 Sample collection, and nutrient and chemical analysis

Along a water level gradient, soil samples were collected at approximately monthly intervals to measure hydrochemical characteristics during the growing season from April 2014 through October 2017 in both wetlands (Fig. 1). The geographical coordinates and the elevation of each site were recorded using a GPS receiver (eTrex Vista; Garmin, New Taipei City, Taiwan, China). A total of 50 sample points were investigated. Soil sampling followed a stratified random sampling design using 0.25 m × 0.25 m quadrats in which soil samples

were excavated at six depths (0–10, 10–20, 20–40, 40–60, 60–80, 80–100, down to the groundwater) with three replicates. Soil samples were transported on ice packs from the field to the lab, where they were aseptically homogenized and stored at 4°C until they could be analyzed. The bulk density was measured in each layer using a bulk soil sampler (5 cm in diameter and 5 cm in height, with a stainless-steel cutting ring). The soil particle-size distribution was measured using a Mastersizer 2000 Laser Particle Size Analyzer (Malvern Scientific Instruments, Malvern, UK). Soil samples were air-dried, passed through a 0.25-mm sieve, and then homogenized before the soil nutrient and chemical analysis.

EC was also measured using a DDS-307 salinity meter (Boqu Scientific Instruments, Shanghai, China), and the pH was measured using an 868 pH meter (Orion Scientific Instruments, MN, USA). The TN, TC, and SOM concentrations were measured with a Vario EL III Elemental Analyzer (Elementar Scientific Instruments, Hanau, Germany). TP was determined by means of perchloric-acid digestion followed by ammonium-molybdate colorimetry using a UV-2450 spectrophotometer (Shimadzu Scientific Instruments, Kyoto, Japan). AN was determined using the alkalizable diffusion method. AP was determined with a spectrophotometer after extraction using bicarbonate solution. AK was determined with a flame photometer. The carbonate (CO_3^{2-}) and bicarbonate ions (HCO_3^-) were measured using the double-indicator neutralization method; Chloride (Cl^-) and sulfate (SO_4^{2-}) were measured using ion chromatography. Major cation concentrations, including dissolved calcium (Ca^{2+}), magnesium (Mg^{2+}), potassium (K^+), and sodium (Na^+), were measured using an inductively coupled plasma-atomic emission spectrometer and atomic absorption spectrometry.

We measured the density of total carbon (*TCD*), total nitrogen (*TND*), and total phosphorus (*TPD*) to a depth of 100 cm using the following equation:

$$SOCD = \sum_{i=1}^{n} \frac{C_i \times \rho_b \times d_i}{100} \qquad (9)$$

where *SOCD* represents *TCD*, *TND*, or *TPD* to a depth of 100 cm (kg/m^2); *i* is the depth of a soil layer; C_i is the content of TC, TN, or TP (g/kg) in that layer; ρ_b is the soil bulk density (g/cm^3); and d_i is the thickness of the soil layer (cm).

3.3 Statistical analysis

We evaluated the model's ability to fit the field-measured values (Camino-Serrano et al., 2014) in both wetlands using three statistical parameters: the absolute mean error (AME), the root-mean-square error (*RMSE*), and the model goodness of fit (R^2). These indices were calculated as follows:

$$AME = \frac{1}{n}\sum_{i=1}^{n}(P_i - M_i) \quad (10)$$

$$RMSE = \sqrt{\frac{1}{n}\sum_{i=1}^{n}(P_i - M_i)^2} \quad (11)$$

$$R^2 = 1 - \frac{\sum_{i=1}^{n}(P_i - M_i)^2}{\sum_{i=1}^{n}(P_i - \bar{M}_i)^2} \quad (12)$$

where P_i, M_i, and $\bar{M}$ are the predicted, observed, and mean values of the observations.

Canonical correspondence analysis (CCA) is a form of direct gradient analysis that measures the environmental gradient directly, and is thus appropriate for studies that focus on examining the relationships between soil properties and environmental variables. We therefore used CCA to provide an ordination for the relationships among the environmental factors and the soil properties. We performed the CCA using Canoco 4.5 to explore the relationships among *TCD*, *TND*, and *TPD* and the soil hydrochemical characteristics (SOM, TN, TC, TP, AN, AP, AK, SO_4^{2-}, Cl^-, HCO_3^-, Ca^{2+}, Mg^{2+}, K^+, Na^+, pH, and *EC*) during the measurement period. As in CCA, each axis has an eigenvalue that indicates its importance, with positive eigenvalues, corresponding to patterns of positive spatial correlation, because

the eigenvalues represent the variance explained on the corresponding principal coordinates and this variance. The sum of all eigenvalues is close to 1.0, and starting from the first axis, the importance of principal coordinates decreases in the order of their decreasing eigenvalues. The intra-set correlations represent the contribution of the explained variation to each axis, with the higher the value, the greater the correlation between variation and axis. We also analyzed the significance of the effects of the wetland type, soil depth, time, and their interactions on soil hydrochemical characteristics (SOM, TN, TC, TP, AN, AP, AK, SO_4^{2-}, Cl^-, HCO_3^-, Ca^{2+}, Mg^{2+}, K^+, Na^+, pH, and *EC*) by means of using repeated-measures ANOVA to compare the main effects and the interactive effects, and considered values to be significantly different when $P < 0.05$. We performed this analysis using version 13.0 of the SPSS software (https://www.ibm.com/analytics/spss-statistics-software).

4. Results

4.1 Meteorological and hydrological processes

During the study period, annual precipitation averaged 124.5±12.4 mm from 2014 to 2017. Most precipitation events were less than 5 mm, and summer events accounted for more than 60% of annual precipitation. *ET* increased from May to July and then decreased to its minimum value in October; for the saltmarsh and riparian wetlands (respectively), *ET* averaged 660.23 and 587.94 mm yr^{-1}, versus simulated values of 672.94 and 627.82 mm yr^{-1}(Fig. 2A). Groundwater depth (Fig. 2B) showed obvious seasonal variation in the saltmarsh wetland, whereas groundwater depth fluctuated but remained near the average value in the riparian wetland. Groundwater depth averaged 130.87±14.55 cm in the saltmarsh wetland and 85.57±5.57 cm in the riparian wetland, versus simulated values of 131.70±12.37 cm and 84.82±4.81 cm (Fig. 2B). During the freezing period, the moisture content near the soil surface decreased significantly, but there was only a small change in the deeper layers. During the study period, the soil moisture increased gradually with increasing depth in the soil. The soil moisture at depths of 10, 20, 40, 60, and 80 cm averaged 24, 25, 27, 34, and 37%, respectively, in the saltmarsh wetland, versus 26, 27, 28, 32, and 39% in the riparian

wetland (Fig. 2C). During the study period, soil salinity had annual averages of 29.80 g kg^{-1} in the riparian wetland, where it showed relatively small fluctuations over time, versus and 63.64 g kg^{-1} in the saltmarsh wetland, which showed dramatic seasonal changes (Fig. 2D). During the freezing period, the surface salt content decreased because the soil was frozen, but the surface salinity gradually increased, and salt accumulation and precipitation occurred near the soil surface, as the soil thawed. R_n, G, λET, and H showed clear seasonal and inter-annual variability, with a unimodal curve. In the saltmarsh wetland, annual values of these parameters averaged 7.48±5.06 $MJ \cdot m^{-2} \cdot d^{-1}$ for R_n, 0.91±2.39 $MJ \cdot m^{-2} \cdot d^{-1}$ for G, 5.13±4.02 $MJ \cdot m^{-2} \cdot d^{-1}$ for λET, and 1.46±1.38 $MJ \cdot m^{-2} \cdot d^{-1}$ for H (Fig. 2E). In the riparian wetland, the corresponding values were 6.83±5.45 $MJ \cdot m^{-2} \cdot d^{-1}$ for R_n, -0.05±0.78 $MJ \cdot m^{-2} \cdot d^{-1}$ for G, 3.62±4.12 $MJ \cdot m^{-2} \cdot d^{-1}$ for λET, and 3.24±3.10 $MJ \cdot m^{-2} \cdot d^{-1}$ for H (Fig. 2F).

[Fig. 2. near here]

4.2 Hydrochemical characteristics

4.2.1 Hydrochemical characteristics

The soil samples revealed a clear trend towards higher SO_4^{2-}, Na^+, Ca^{2+}, and Cl^-fractions as well as lower Mg^{2+}, K+, and HCO_3^- fractions in both wetlands (Fig. 3). Among the cations, Na^+ and Ca^{2+} were dominant in both wetlands. Among the anions, which come primarily from groundwater, SO_4^{2-} and Cl^- were dominant in both wetlands. Therefore, the major ion types were Na^+-Ca^{2+}-SO_4^{2-}-Cl^- in the saltmarsh wetland and the riparian wetland, respectively.

[Fig. 3. near here]

4.2.2 Variation of major ion and nutrient concentrations

The major ion concentrations showed changes similar to the seasonal variation of hydrological characteristics during the study period (Fig. 4). The concentrations decreased from a maximum in April to a minimum in June, and then increased until September. During

the freezing period, the major ions that were trapped in frozen water exhibited desalination during the crystallization process. However, the ions were gradually released during the melting period, in April, and combined with salt accumulation and precipitation near the soil surface, accompanied by continuous *ET*. However, the ion concentrations decreased significantly as the water level approached the surface, accompanied by dilution caused by precipitation during the rainy season. As *ET* continued during the growing season, water flux started to move upward to compensate for the water loss near the soil surface. Consequently, the accumulation of major ions in the upper soil layer occurred again, and a crust formed at the surface that allowed more ions to accumulate below the crust. Therefore, a second peak occurred in July when ET was at its highest value.

[Fig. 4. near here]

We found no significant seasonal change in the nutrient concentrations; the nutrient concentrations fluctuated, but remained near the overall mean for the growing season (Fig. 5). In the saltmarsh wetland, the measured values averaged 10.15±0.82 g/kg for SOM, 0.80±0.06 g/kg for TN, 28.22±1.50 g/kg for TC, 1.52±0.08 g/kg for TP, 37.82±2.83 mg/kg for AN, 4.20±0.25 mg/kg for AP, and 379.92±24.80 mg/kg for AK. In the riparian wetland, they averaged 6.31±0.42 g/kg for SOM, 0.46±0.03 g/kg for TN, 11.83±0.67 g/kg for TC, 1.57±0.07 g/kg for TP, 24.27±1.47 mg/kg for AN, 4.32±0.19 mg/kg for AP, and 205.25±15.18 mg/kg for AK.

[Fig. 5. near here]

The differences between simulated and measured values for the ion and nutrient concentrations were generally small in both wetlands (Fig. 4, 5). In the saltmarsh wetland, RMSE ranged from 0.016 to 0.925 g/kg for the major ions (Fig. 4) and from 0.305 mg/kg to 1.010 g/kg for the nutrients (Fig. 5). In the riparian wetland, RMSE ranged from 0.008 to 0.460 g/kg for the major ions (Fig. 4) and from 0.449 mg/kg to 0.871 g/kg for the nutrients (Fig. 5).

Figure 6 shows the trends for the ion concentrations as a function of depth in the soil. In both wetlands, the major ion concentrations decreased significantly ($p< 0.05$) with increasing depth in the soil. However, there were no significant differences among the values at depths of 60 to 100 cm ($p> 0.05$). In both wetlands, the linear regressions for the relationships between the measured and predicted values were all strong and significant for the major ions (Fig. 6; $R^2> 0.97$, $P< 0.05$) and for the nutrients (Fig. 7, $R^2> 0.93$, $P< 0.05$). In the saltmarsh wetland, RMSE ranged from 0.008 to 0.236 g/kg for the major ions (Fig. 6). In the riparian wetland, RMSE ranged from 0.012 to 1.364 g/kg for the major ions (Fig. 6). These results indicated high accuracy of the prediction of major ion and nutrient concentrations for the two wetlands.

[Fig. 6. near here]

The nutrient concentrations also decreased significantly ($P < 0.05$) with increasing depth in the soil (Fig. 7). The nutrient concentrations of saltmarsh wetland was significantly higher than that of riparian wetland, and the nutrient concentrations to a depth of 100 cm ranged from5.8±0.32 to 10.64±0.67 g/kg for SOM, from 0.43±0.02 to 0.78±0.04 g/kg for TN, from 12.1±0.51 to27.68±1.66 g/kg for TC, from 1.14±0.02 to 1.33±0.03 g/kg for TP, from 22.96±1.18 to 39.85±2.19 mg/kg for AN, from 5.09±0.28 to 6.12±0.16 mg/kg for AP, and 173±10.6 and 386.42±15.39 mg/kg for AK in the riparian wetland and saltmarsh wetland, respectively. In the saltmarsh wetland, RMSE ranged from 1.120 mg/kg to 1.071 g/kg for the nutrients (Fig. 7). In the riparian wetland, RMSE ranged from 0.079 mg/kg to 2.140 g/kg for the nutrients (Fig. 7).

[Fig. 7. near here]

The linear regressions for the relationships between the simulated and measured values produced strong ($R^2> 0.93$) and statistically significant ($P< 0.05$) results for both wetlands. Thus, the model did a good job of predicting both major ion and nutrient concentrations. The

goodness of fit was stronger for the Hydrus-1D model (i.e., for the ions) than for the DNDC model (i.e., for the nutrients). Nonetheless, both model fits were generally excellent.

4.2.3 Density and storage of total C, N, and P

TCD, *TND*, and *TPD* were higher in the saltmarsh wetland than in the riparian wetland at all depths in the soil (Table 3). In the saltmarsh wetland, the values were 6.18±3.51 kg·m^{-2} for *TCD*, 0.18±0.10 kg·m^{-2} for *TND*, and 0.29±0.14 kg·m^{-2} for *TPD*, versus 1.96±0.79 kg·m^{-2} for *TCD*, 0.08±0.03 kg·m^{-2} for *TND*, and 0.22±0.09 kg·m^{-2} for *TPD* in the riparian wetland. The maximum values of *TCD*, *TND*, and *TPD* were at 50 to 80 cm below the surface in the saltmarsh wetland, versus 30 to 50 cm in the riparian wetland. In both wetlands, *TCD*, *TND*, and *TPD* were higher at 50 to 100 cm below the surface than in the top 50 cm of the soil. This indicates a stronger sink function for C, N, and P deeper in the soil.

[Table 3. near here]

The storage of total carbon (*STC*), total nitrogen (*STN*), and total phosphorus (*STP*) in the saltmarsh wetland were higher than those in the riparian wetland (Fig. 8). In the saltmarsh wetland, average total storage was 372.72±66.52 t C/hm^2 for *STC*,10.92±2.59 t N/hm^2 for *STN*, and 17.55±1.54 t P/hm^2 for *STP*, versus 119.72±27.88 t C/hm^2, 4.38±1.24 t N/hm^2, and 13.17±1.46 t P/hm^2, respectively, in the riparian wetland. All three storage values increased with the increase of soil salinity in the saltmarsh wetland, which indicates that wetland salinization can increase nutrient storage.

[Fig. 8. near here]

4.3 Effects of hydrochemical characteristics on soil C, N, and P

4.3.1 Effects and their interactions on hydrochemical characteristics

Table 4 summarizes the significance of the effects of wetland type (WT), soil depth (SD), sampling time (ST), and their interactions (WT × SD,WT × ST,SD × ST,WT × SD × ST) on the hydrochemical characteristics (SOM, TN, TC, TP, AN, AP, AK, *TCD*, *TND*, *TPD*,

SO_4^{2-}, Cl^-, HCO_3^-, Ca^{2+}, Mg^{2+}, K^+, Na^+, N:K, C:P, C:K, C:N, *EC*). The F value is the ratio of two mean squares (effect term/error term). The larger the F value (compared with the standard F value with a given significance level), the greater the effect difference between the treatments, and the smaller the error term with the higher the test accuracy. The F value shown that the effects in the two arid wetlandswere mostly significant ($P< 0.001$). However, the main effects and their interaction terms did not significantly explain pH during the measuring period, and the volumetric water content (VWC) was only significantly explained by sampling time. Soil C:N, C:P, and N:P ratios all increased with salt accumulation (i.e., were higher in the saltmarsh wetland). The high C:P and N:P < 14 indicated that N and P were the limiting factors for plant growth, and that N was more restricted than P. Therefore, the accumulation of salt in arid wetlands appears to increase *STC*, *STN*, and *STP* during the process of salinization, and this change increases the wetland's function as a sink for C, N, and P, but especially for C.

[Table 4. near here]

4.3.2 Effects of hydrochemical characteristics on soil C, N, and P

We performed CCA to explore the relationships between *TND*, *TCD*, and *TPD* and the hydrochemical characteristics during the measurement period. Table 5 presents the eigenvalues for the first four principal coordinate (PC) axes in the CCA analysis. The correlations between *TCD*, *TND*, and *TPD* and the hydrochemical factors was high for the first three canonical axes (0.760, 0.256 and 0.179, respectively, for the saltmarshwetland, versus0.814, 0.383, and 0.231, respectively, for the riparian wetland), and the combination of *TCD*, *TND*, and *TPD* explained 98.8%of the cumulative variance in the saltmarsh wetland and 98.0% in the riparian wetland (Table 5, Fig. 9). These results suggest a strong association between *TCD*, *TND*, *TPD*, and the hydrochemical parameters. In the intra-set correlation for the hydrochemical factors, the first axis accounted for 80.3and 80.8% of the total variance for the saltmarsh wetland and riparian wetland, respectively, versus 14.5 and 12.5%, respectively,

for the second axis. In addition, Axis 3 is associated with a high negative loading for TN and a moderate loading for pH (Table 5).

[Table 5. near here]

5. Discussion

5.1 Hydrochemical characteristics

The hydrological conditions and chemical characteristics are primary factors that determine a wetland's type, formation mechanism, and persistence (Crosbie et al., 2009; Bijoor et al., 2011; Glenn et al., 2012; Liu et al., 2014, 2019). We found that the nutrient and major ion concentrations gradually decreased with increasing depth below the surface in the saltmarsh and riparian wetlands. These compounds have laid a rich foundation for the formation of carbonates. With continuous *ET*, salts are transported upward toward the soil surface in water that is migrating upward via capillary rise from the shallow groundwater, leading to salt accumulation and concentration increases near the surface (Xu et al., 2014; Liu et al., 2014). At the same time, ion exchange and adsorption occur between soil particles and ions in the groundwater. The $Ca^{2+}+Mg^{2+}/HCO_3^-$ ratio can be used to explain the sources of Mg^{2+} and Ca^{2+} in groundwater. When soil particles adsorb Mg^{2+} and Ca^{2+} from the groundwater, this increases the concentration of Na^+ in the soil solution. Generally, shallow groundwater strongly dilutes ions in the soil solution in riparian wetlands, which is why the ion concentrations are lower than in a saltmarsh wetland (Liu et al., 2014, 2017, 2019). Thus, concentration of the soil solution through *ET* combines with ion adsorption and release to alter hydrochemical characteristics such as the Mg^{2+}/SO_4^{2-} ratio in wetlands. As salinity increases, Ca^{2+} ions are added to the soil solution faster than HCO_3^-, suggesting a carbonate origin for the Ca^{2+} and another source for bicarbonates, probably through dissolution of dolomite.

Long-term irrigation and fertilization in arid regions to sustain irrigated agriculture can significantly increase SOC, Ca^{2+}, and Mg^{2+}, leading to SOC accumulation at rates ranging

from 101 to 202 g C m^{-2} $year^{-1}$, which provides sufficient C, Ca, and Mg sources for the formation of inorganic carbon in farmland (Wang et al., 2014; Su et al., 2018). In arid wetlands, the ions are transported out of oasis farmland through irrigation and leaching. In addition, agricultural non-point source pollution plays a key role in regulating hydrochemical processes in arid wetlands, since irrigation increases N, P, heavy metals, and organic pollutants in the returned irrigation water, leading to deterioration of water quality in the desert oasis wetland (Furi et al., 2011). This phenomenon has an important impact on the water environment of desert oasis wetlands. In agricultural irrigation, the fertilizer use produces sulfates that are a main source of sulfate pollution in rivers, wetlands, and groundwater (Szynkiewicz et al., 2011; Zhou et al., 2016). In the middle reaches of the Heihe River, agricultural fertilizer significantly affects the sulfate isotope composition (Li et al., 2013). In addition, chloride deposition is a key process in salt lakes (Ye et al., 2015). The abovementioned combinations of Ca^{2+} and Na^{+} desorption with the release of SO_4^{2-} and Cl^{-} explain why the major ion type was Na^{+}-Ca^{2+}- SO_4^{2-}-Cl^{-}in the saltmarsh wetland and riparian wetland.

The silicates contain cations, and can decompose to release Ca^{2+} and Mg^{2+}. In addition, the water that flows down from mountain areas transports large quantities of Ca^{2+}, Mg^{2+}, K^{+}, Na^{+}, and other cations (Li et al., 2015a,b; Wu et al., 2016), which improves the soil cation content in the arid wetlands that receive these flows. However, the adsorption of carbonate to soil particles was not considered in previous reports. In an alkaline and calcium-rich geochemical environment with abundant oxygen and a pH of ~8 in an arid wetland in China, CO_2 is generated and it forms a weak acid that can dissolve the deposits of soil inorganic carbon to increase soil organic carbon. This is because the mineralization rate of soil organic matter is high, resulting in the deposition of inorganic carbon. Precipitated carbonates are deposited in deep soil and enter the groundwater layer through leaching; alternatively, heavy rain in mountainous areas and artificial irrigation in oases can transport carbonate to a lake or wetland at the end of a river (Li et al., 2015a,b).

5.2 Density and storage of total C, N, and P

The soil C, N, and P contents depend strongly on the balance between inputs and outputs, which mainly originate from plant and animal residues, and soil microbial biomass, and their stocks depend on the organic matter accumulation and decomposition rates (Schulze et al., 2009; Wu et al., 2016). In the present study, nutrient concentrations fluctuated around an equilibrium point rather than showing a seasonal trend (Fig. 5), but decreased with increasing soil depth in both arid wetlands (Fig. 7). Other researchers have confirmed that the fixation of soil C strongly controls the soil N content, and this explains why the two nutrients show similar trends (Elser et al., 2007).

We also found that *TCD*, *TND*, and *TPD* were higher in the saltmarsh wetland than in the riparian wetland at all depths (Table 3). *TCD*, *TND*, and *TPD* were significantly positively correlated with *TN*, *TC*, and *TP*. The overall C:N ratios for our study area were far lower than the C:N ratios (about 22) in arid wetland. Grassland ecosystems have a lower C:N ratio and a narrower range of ratios because of the faster turnover of SOM. Wu et al. (2016) suggested that *SOC* in arid wetlands usually decomposes more slowly than in grassland ecosystems and thus has a higher C:N ratio. The C:N ratio(27.84) in arid wetlands is higher than the Chinese national average (13, indicating less-decomposed SOM). The average values of C:P (14.76) > N:P (0.53) in the arid wetland soils of our study area, and these are lower than the corresponding national average values (105 and 8, respectively). This indicates that the humus content of soil organic matter is higher than the national average, and that organic N and P are more easily mineralized. At the same time, high C, N, and P also mean that there may be little exchange of soil nutrients between the arid wetlands and their external environment. Saline wetlands in arid regions, the irrigation backwater is also one of the main water sources which are rich in salt ions and nutrient elements bacause of fertilizer application in agricultural activity (Liu et al., 2014, 2017, 2019). On the one hand, salt ions and nutrient elements are transported towards the soil surface through capillary rise from shallow groundwater and irrigation water with continuous evapotranspiration, leading to salt

accumulation and nutrient enrichment near the soil surface (Xu et al., 2005, 2013). This eventually leads to a significant increase in soil TC, TN, and TP during the process of wetland salinization, the increase continues. On the other hand, seasonal and interannual variability in river runoff affects the freshwater discharge into wetlands and influences the processes of hydrochemical characteristics, organic matter accumulation and decomposition processes. After salinization of a wetland, the oxygen supply was insufficient in anaerobic environment, the microorganism quantity and the enzyme activity were inhibited in soil, the organic matter that was present decomposes slower than before salinization occurred, leading to the increased TN, whereas STC, STN, and STP increased with the increase of salinity in the saltmarsh wetland, which indicates that wetland salinization can improve the wetland's function as a sink for C and N, although this differs from the results of Huo et al. (2013) and Wu et al. (2016).

In addition, CO_2 absorbed by water in alkali and saline wetlands forms a weak acid that can leach into the groundwater and promote the dissolution of carbonates, thereby decreasing the C sink potential (Li et al., 2015a; Wu et al., 2016). In the Mojave Desert, Gurbantunggut Desert, and Badain Jaran Desert, where the ecosystem absorbed more than 100 g C m^{-2} $year^{-1}$ (Jasoni et al., 2005; Xie et al., 2009), the TCD of the desert saline soil is even greater. ^{13}C tracer studies showed that atmospheric CO_2 can directly enter a desert soil and become bound to the soil particles (Wohlfahrt et al., 2015); as a result, soils of desert and semi-arid areas were estimated to absorb of 5.2 Pg C $year^{-1}$ as CO_2, amounting to global soil carbon reserves of 551 Pg C, of whichsoil inorganic carbon reserves accounted for 83% (Stone, 2008; Ma et al., 2014; Liu et al., 2015a). The storage of *TC* to a depth of 1 m that was observed in a previous study of an arid region would take 106 years to accumulate (Su et al., 2018). However, the storage of *TC* was 37.2 kg C m^{-2} to a depth of 1 m in the saltmarsh wetland, and it would take 372 years for this level of *TC* to accumulate at a rate of 100 g C $m^{-2}year^{-1}$.

5.3 Effects of hydrochemical characteristics on soil C, N, and P

In the saltmarsh wetland, this axis was positively correlated with the concentrations of *SOC*, *TN*, *AN*, *AK*, SO_4^{2-}, Cl^-, Ca^{2+}, Mg^{2+}, K^+, Na^+, pH, and *EC* (Fig. 9a). This particular pattern, combined with high positive loadings for the hydrochemical factors (Table 5), may reflect the influence of fertilizer and pesticide application on pollution of the groundwater, and may therefore represent agricultural non-point source pollution. The strong positive loadings for Ca^{2+}, Mg^{2+}, and *EC* probably cannot be attributed directly to salinizationof the soil, but rather to secondary processes such as ion exchange, which become more evident in more salinized soils (Fig. 9).

[Fig. 9 near here]

In the saltmarsh wetland (Fig. 9A), the second axis was negatively correlated with HCO_3^-, *AP*, *TP*, *TC*, *TCD*, *TPD*, *SOC*, *TND*, *TN*, and pH. This results from dilution of the groundwater by water recharge or mineralization caused by interactions between water, soil, and rocks. In the riparian wetland (Fig. 9B), the second axis was negatively correlated with HCO_3^-, *AP*, *TP*, *TC*, *TCD*, *TPD*, *SOC*, *TND*, and *TN*. The fresh water provided by precipitation or recharge of the aquifer by river water during the sampling period dissolves carbonate rocks (Li et al., 2015a; Wu et al., 2016). In addition, the presence of carbonate rocks such as calcite and dolomite in the river sediments causes the HCO_3^- concentration to increase throughout the aquifer (Su et al., 2018). The negative loading for pH may be caused by the biogenic or organic control of pH by river sediments. In addition, NO_3^- pollution is serious in our study area because of extensive agricultural activity in the region, combined with nitrate in domestic wastewater (Ma et al., 2014; Liu et al., 2017; Liu et al., 2019). An inverse relationship between TN and pH represents nitrification. Through nitrification, *TN* is enriched, and H^+ is produced as a byproduct, leading to a decrease of groundwater pH.

6 Conclusions

Until the present study, there was little knowledge about the relationships between hydrochemical characteristics, the source/sink function, and C, N, and P cycling in wetlands

in arid regions. In the present study, the major ion type was Na^{+}-Ca^{2+}-SO_4^{2-}-Cl^{-} in the saltmarsh wetland and riparian wetland. The anion, cation, and nutrient concentrations decreased gradually but significantly with increasing depth in the soil in both wetlands, which suggests that fertilizer and pesticide application in local farmland led to groundwater pollution that plays a key role in regulating hydrochemical processes, and also suggests that the agricultural irrigation increases levels of N and P in the wetlands. Desert soil has a high sand content, and dissolution of the particles and release of bound cations by weak acids improves the soil cationic content in the arid wetlands. In addition, precipitated carbonates were deposited in the deep soil and were leached into the groundwater layer by weak acids. The storage of total carbon to a depth of 1 m reached 37.2 kg C m^{-2} in the saltmarsh wetland, which would take 372 years to accumulate at a rate of 100 g C m^{-2} $year^{-1}$. Evapotranspiration and concentration processes and ion adsorption to soil particles strongly affected the hydrochemical characteristics of the wetlands. As salinity increased, Na^{+} and Ca^{2+} were added to the soil solution at a greater rate than HCO_3^{-}, suggesting a carbonate origin for the calcium and another source (probably dolomite) for bicarbonates.

Acknowledgments

This study was supported by the key project of the National Natural Science Foundation of China (No. 41630861), by the National Key Research and Development Program of China (no. 2017YFC0504306), and by the National Natural Science Foundation of China (Nos. 41771038; 41807150). We thank all the participants in the vegetation and environmental surveys conducted at the Linze Inland River Basin Research Station, Cold and Arid Regions Environmental and Engineering Research Institute, Chinese Academy of Sciences. We also gratefully acknowledge the journal's anonymous reviewers for their valuable comments on an earlier version of our manuscript. The authors declare noconflict of interests.Data for this manuscript are available at Figshare (https://doi.org/10.6084/m9.figshare.11913990).

References

Bijoor, N.S., Pataki, D.E., Rocha, A.V., Goulden, M.L. (2011). The application of $\delta^{18}O$ and δD for understanding water pools and fluxes in a *Typhamarsh*. *Plant Cell Environment*, 34, 1761–1775. doi.org/10.1111/j.1365-3040.2011.02372.x

Busscher, W. (1980). Simulation of field water use and crop yield. *Soil Science*, *129*(3), 193. doi.org/10.1097/00010694-198003000-00016

Camino-Serrano, M., Gielen, B., Luyssaert, S., Ciais, P., Vicca, S., Guenet, B., Vos, B. D., Cools, N., Ahrens, B., Arain, M. A., Borken, W., Clarke, N., Clarkson, B., Cummins, T., Don, A., Pannatier, E. G., Laudon, H., Moore, T., Nieminen, T. M., Nilsson, M. B., Peichl, M., . Schwendenmann, L., Siemens, J.,& Janssens, I. (2014). Linking variability in soil solution dissolved organic carbon to climate, soil type, and vegetation type. *Global Biogeochemical Cycles*, 28(5), 497-509.doi.org/10.1002/2013GB004726

Castañeda, C., & Herrero, J. (2008). Assessing the degradation of saline wetlands in an arid agricultural region in Spain. *Catena*, *72*(2), 205–213. doi.org/10.1016/j.catena.2007.05.007

Chambers, L. G., Osborne, T. Z., & Reddy, K. R. (2013). Effect of salinity-altering pulsing events on soil organic carbon loss along an intertidal wetland gradient: a laboratory experiment. *Biogeochemistry*, *115*(1–3), 363–383. doi.org/10.1007/s10533-013-9841-5

Chambers, L. G., Reddy, K. R., & Osborne, T. Z. (2011). Short-term response of carbon cycling to salinity pulses in a freshwater wetland. *Soil Science Society of America Journal*, *75*(5), 2000–2007. doi.org/10.2136/sssaj2011.0026

Cheng, X., Luo, Y., Xu, Q., Lin, G., Zhang, Q., Chen, J., & Li, B. (2010). Seasonal variation in CH_4 emission and its ^{13}C-isotopic signature from *Spartina alterniflora* and *Scirpusmariqueter* soils in an estuarine wetland. *Plant and Soil*, *327*(1), 85–94. doi.org/10.1007/s11104-009-0033-y

Couto, T., Duarte, B., Caçador, I., Baeta, A., & Marques, J. C. (2013). Salt marsh plants carbon storage in a temperate Atlantic estuary illustrated by a stable isotopic analysis based approach. *Ecological Indicators*, *32*, 305–311. doi.org/10.1016/j.ecolind.2013.04.004

Crosbie, R.S., McEwan, K.L., Jolly, I.D., Holland, K.L., Lamontagne, S., Grotthing Moe, K., Simmons, C.T. (2009). Salinization risk in semi-arid floodplain wetlands subjected to engineered wetting and drying cycles. *Hydrological Process*, 23, 3440–3452. doi.org/10.1002/hyp.7445

Cui, G., & Wang, J. (2019). Improving the DNDC biogeochemistry model to simulate soil temperature and emissions of nitrous oxide and carbon dioxide in cold regions. *Science of the Total Environment*, *687*, 61–70. doi.org/10.1016/j.scitotenv.2019.06.054

Deng, J., Zhu, B., Zhou, Z., Zheng, X., Li, C., Wang, T., & Tang, J. (2011). Modeling nitrogen loadings from agricultural soils in southwest China with modified DNDC. *Journal of Geophysical Research: Biogeosciences*, *116*(2). doi.org/10.1029/2010JG001609

Drexler, J. Z., Krauss, K. W., Sasser, M. C., Fuller, C. C., Swarzenski, C. M., Powell, A. (2013). A long-term comparison of carbon sequestration rates in impounded and naturally tidal freshwater marshes along the Lower Waccamaw River, South Carolina. *Wetlands*, *33*(5), 965–974. doi.org/10.1007/s13157-013-0456-3

Elser, J. J., Bracken, M. E. S., Cleland, E. E., Gruner, D. S., Harpole, W. S., Hillebrand, H., et al. (2007). Global analysis of nitrogen and phosphorus limitation of primary producers in freshwater, marine and terrestrial ecosystems. *Ecology Letters*, *10*(12), 1135–1142. doi.org/10.1111/j.1461-0248.2007.01113.x

Feng, Z. T., Deng, Y. Q., Fan, H., Sun, Q. J., Sui, N., & Wang, B. S. (2014). Effects of NaCl stress on the growth and photosynthetic characteristics of *Ulmuspumila* L. seedlings in sand culture. *Photosynthetica*, *52*(2), 313–320. doi.org/10.1007/s11099-014-0032-y

Finger, R.A., Turetsky, M.R., Kielland, K., Ruess, R.W., Mack, M.C., & Euskirchen, E.S.(2016) Effects of permafrost thaw on nitrogen availability and plant–soil interactions in a boreal Alaskan lowland. *Journal of Ecology*, 104(6), 1542–1554. doi.org/ doi.org/10.1111/gcb.12431

Furi, W., Razack, M., Haile, T., Abiye, T. A., & Legesse, D. (2011). The hydrogeology of Adama-Wonji basin and assessment of groundwater level changes in Wonji wetland, Main Ethiopian Rift: results from 2D tomography and electrical sounding methods. *Environmental Earth Sciences*, *62*(6), 1323–1335. doi.org/10.1007/s12665-010-0619-y

Giltrap, D. L., Li, C., & Saggar, S. (2010). DNDC: a process-based model of greenhouse gas fluxes from agricultural soils. *Agriculture, Ecosystems and Environment*, *136*(3–4), 292–300. doi.org/10.1016/j.agee.2009.06.014

Glenn, E.P., Mexicano, L., Garcia-Hernandez, J., Nagler, P.L., Gomez-Sapiens, M.M., Tang, D.A., Lomeli, M.A., Ramirez-Hernandez, J., Zamora-Arroyo, F., 2012. Evapotranspiration and water balance of an anthropogenic coastal desert wetland:responses to fire, inflows and salinities. Ecological. Engneer. 59 (5), 176–184.

Gran, M., Carrera, J., Massana, J., Saaltink, M. W., Olivella, S., Ayora, C., & Lloret, A. (2011). Dynamics of water vapor flux and water separation processes during evaporation from a salty dry soil. *Journal of Hydrology*, *396*(3–4), 215–220. doi.org/10.1016/j.jhydrol.2010.11.011

Huckelbridge, K. H., Stacey, M. T., Glenn, E. P., & Dracup, J. A. (2010). An integrated model for evaluating hydrology, hydrodynamics, salinity and vegetation cover in a coastal desert wetland. *Ecological Engineering*, *36*(7), 850–861. doi.org/10.1016/j.ecoleng.2010.03.001

Huo, L., Chen, Z., Zou, Y., Lu, X., Guo, J., & Tang, X. (2013). Effect of Zoige alpine wetland degradation on the density and fractions of soil organic carbon. *Ecological Engineering*, *51*, 287–295. doi.org/10.1016/j.ecoleng.2012.12.020

Jasoni, R. L., Smith, S. D., & Arnone, J. A. (2005). Net ecosystem CO_2 exchange in Mojave Desert shrublands during the eighth year of exposure to elevated CO_2. *Global Change Biology*, *11*(5), 749–756. doi.org/10.1111/j.1365-2486.2005.00948.x

Johnson, W. C., Millett, B. V., Gilmanov, T., Voldseth, R. A., Guntenspergen, G. R., & Naugle, D. E. (2005). Vulnerability of northern prairie wetlands to climate change. *BioScience*, *55*(10), 863. doi.org/10.1641/0006-3568(2005)055[0863:vonpwt]2.0.co;2

Jolly, I. D., McEwan, K. L., & Holland, K. L. (2008). A review of groundwater-surface water interactions in arid/semi-arid wetlands and the consequences of salinity for wetland ecology. *Ecohydrology*, *1*(1), 43–58. doi.org/10.1002/eco.6

Juszczak, R., & Augustin, J. (2013). Exchange of the greenhouse gases methane and nitrous oxide between the atmosphere and a temperate peatland in central Europe. *Wetlands*, *33*(5), 895–907. doi.org/10.1007/s13157-013-0448-3

Lafleur, P. M. (2008). Connecting atmosphere and wetland: energy and water vapour exchange. *Geography Compass*, *2*(4), 1027–1057. doi.org/10.1111/j.1749-8198.2007.00132.x

Lamers, L. P. M., Govers, L. L., Janssen, I. C. J. M., Geurts, J. J. M., Van der Welle, M. E. W., Van Katwijk, M. M., et al. (2013). Sulfide as a soil phytotoxin—a review. *Frontiers in Plant Science*. doi.org/10.3389/fpls.2013.00268

Li, C.S., Frolking, S., & Frolking, T. A. (1992). A model of nitrous oxide evolution from soil driven by rainfall events: 1. Model structure and sensitivity. *Journal of Geophysical Research*, *97*(D9), 9759–9776. doi.org/10.1029/92jd00509

Li, C., Frolking, S., Xiao, X., Moore, B., Boles, S., Qiu, J., et al. (2005). Modelling impacts of farming management alternatives on CO_2, CH_4 and N_2O emissions: a case study for water management of rice agriculture of China. *Global Biogeochemical Cycles*, *19*(3), 1–10. doi.org/10.1029/2004GB002341

Li, C., Salas, W., DeAngelo, B., & Rose, S. (2006). Assessing alternatives for mitigating net greenhouse gas emissions and increasing yields from rice production in China over the next twenty years. *Journal of Environmental Quality*, 35,1554–1565. doi.org/10.2134/jeq2005.0208

Li, C., Salas, W., Zhang, R., Krauter, C., Rotz, A., & Mitloehner, F. (2012). Manure-DNDC: a biogeochemical process model for quantifying greenhouse gas and ammonia emissions from livestock manure systems. *Nutrient Cycling in Agroecosystems*, *93*(2), 163–200. doi.org/10.1007/s10705-012-9507-z

Li, H., Wang, L., Li, J., Gao, M., Zhang, J., Zhang, J.F., et al. (2017a). The development of China-DNDC and review of its applications for sustaining Chinese agriculture. *Ecological Modelling*. doi.org/10.1016/j.ecolmodel.2017.01.003

Li, S., & Zhao, W. (2010). Landscape pattern changes of desert oasis wetlands in the middle reach of the Heihe River, China. *Arid Land Research and Management*, *24*(3), 253–262. doi.org/10.1080/15324981003741707

Li, Xi, Ishikura, K., Wang, C., Yeluripati, J., & Hatano, R. (2015a). Hierarchical Bayesian models for soil CO_2 flux using soil texture: a case study in central Hokkaido, Japan. *Soil Science and Plant Nutrition*, *61*(1), 116–132. doi.org/10.1080/00380768.2014.978728

Li, X.Q., Gan, Y., Zhou, A., Liu, Y., & Wang, D. (2013). Hydrological controls on the sources of dissolved sulfate in the Heihe River, a large inland river in the arid northwestern China, inferred from S and O isotopes. *Applied Geochemistry*, *35*, 99–109. doi.org/10.1016/j.apgeochem.2013.04.001

Li, Y., Wang, Y. G., Houghton, R. A., & Tang, L. S. (2015b). Hidden carbon sink beneath desert. *Geophysical Research Letters*, *42*(14), 5880–5887. doi.org/10.1002/2015GL064222

Li, Z., Yang, J. Y., Drury, C. F., Yang, X. M., Reynolds, W. D., Li, X., & Hu, C. (2017b). Evaluation of the DNDC model for simulating soil temperature, moisture and respiration from monoculture and rotational corn, soybean and winter wheat in Canada. *Ecological Modelling*, *360*, 230–243. doi.org/10.1016/j.ecolmodel.2017.07.013

Liu, B., Guan, H., Zhao, W., Yang, Y., & Li, S. (2017). Groundwater facilitated water-use efficiency along a gradient of groundwater depth in arid northwestern China. *Agricultural and Forest Meteorology*, *233*, 235–241. doi.org/10.1016/j.agrformet.2016.12.003

Liu, B., Zhao, W., Wen, Z., & Zhang, Z. (2014). Response of water and energy exchange to the environmental variable in a desert-oasis wetland of Northwest China. *Hydrological Processes*, *28*(25), 6098–6112. doi.org/10.1002/hyp.10098

Liu, B., Zhao, W., Yang, Y., & Li, S. (2019). Mechanisms and feedbacks for evapotranspiration-induced salt accumulation and precipitation in an arid wetland of China. *Journal of Hydrology*, *568*, 403–415.https://doi.org/10.1016/j.jhydrol.2018.11.004

Liu, J., Fa, K., Zhang, Y., Wu, B., Qin, S., & Jia, X. (2015b). Abiotic CO_2 uptake from the atmosphere by semiarid desert soil and its partitioning into soil phases. *Geophysical Research Letters*, *42*(14), 5779–5785. doi.org/10.1002/2015GL064689

Ma, J., Liu, R., Tang, L. S., Lan, Z. D., & Li, Y. (2014). A downward CO_2 flux seems to have nowhere to go. *Biogeosciences*, *11*(22), 6251–6262. doi.org/10.5194/bg-11-6251-2014

Marks, B. M., Chambers, L., & White, J. R. (2016). Effect of fluctuating salinity on potential denitrification in coastal wetland soil and sediments. *Soil Science Society of America Journal*, *80*(2), 516–526. doi.org/10.2136/sssaj2015.07.0265

Morrissey, E.M., Gillespie, J.L., Morina, J.C., & Franklin, R.B.(2014). Salinity affects microbial activity and soil organic matter content in tidal wetlands. *Global Change Biology*, 20, 1351–1362. doi.org/10.1111/gcb.12431

Neubauer, S. C. (2013). Ecosystem responses of a tidal freshwater marsh experiencing saltwater intrusion and altered hydrology. *Estuaries and Coasts, 36*(3), 491–507. doi.org/10.1007/s12237-011-9455-x

Nielsen, D. L., Brock, M. A., Rees, G. N., & Baldwin, D. S. (2003). Effects of increasing salinity on freshwater ecosystems in Australia. *Australian Journal of Botany*, 51,655–665. doi.org/10.1071/BT02115

Noe, G. B., Krauss, K. W., Lockaby, B. G., Conner, W. H., & Hupp, C. R. (2013). The effect of increasing salinity and forest mortality on soil nitrogen and phosphorus mineralization in tidal freshwater forested wetlands. *Biogeochemistry*, *114*(1–3), 225–244. doi.org/10.1007/s10533-012-9805-1

Page, K. L., & Dalal, R. C. (2011). Contribution of natural and drained wetland systems to carbon stocks, CO_2, N_2O, and CH_4 fluxes: an Australian perspective. *Soil Research*, 49(5), 377-388. doi.org/10.1071/SR11024

Pathak, H., Li, C., & Wassmann, R. (2005). Greenhouse gas emissions from Indian rice fields: calibration and upscaling using the DNDC model. *Biogeosciences Discussions*, *2*(1), 77–102. doi.org/10.5194/bgd-2-77-2005

Pont, D., Simonnet, J. P., & Walter, A. V. (2002). Medium-term changes in suspended sediment delivery to the ocean: consequences of catchment heterogeneity and river management (Rhône River, France). *Estuarine, Coastal and Shelf Science*, *54*(1), 1–18. doi.org/10.1006/ecss.2001.0829

Saito, H., Šimůnek, J., Mohanty, B., 2006. Numerical analysis of coupled water, vapor,and heat transport in the vadose zone. *Vadose Zone Journal*, 5 (2), 784–800.doi.org/10.2136/vzj2006.0007

Schulze, K., Borken, W., Muhr, J., & Matzner, E. (2009). Stock, turnover time and accumulation of organic matter in bulk and density fractions of a Podzol soil. *European Journal of Soil Science, 60*(4), 567–577. doi.org/10.1111/j.1365-2389.2009.01134.x

Šimůnek, J., Van Genuchten, M. T., & Sejna, M. (2013). The HYDRUS Software Package for Simulating the Two- and Three-Dimensions Movement of Water, Heat, and Multiple Solutes in Variably-Saturated Media. *Technical Manual*. doi.org/10.1007/SpringerReference_28001

Song, C., Xu, X., Tian, H., & Wang, Y. (2009). Ecosystem-atmosphere exchange of CH_4 and N_2O and ecosystem respiration in wetlands in the Sanjiang Plain, Northeastern China. *Global Change Biology*, *15*(3), 692–705. doi.org/10.1111/j.1365-2486.2008.01821.x

Sperling, O., Lazarovitch, N., Schwartz, A., & Shapira, O. (2014). Effects of high salinity irrigation on growth, gas-exchange, and photoprotection in date palms (*Phoenix dactylifera* L., cv. Medjool). *Environmental and Experimental Botany*, *99*, 100–109. doi.org/10.1016/j.envexpbot.2013.10.014

Stone, R. (2008). Ecosystems: have desert researchers discovered a hidden loop in the carbon cycle?*Science*, 320(5882), 1409-1410. doi.org/10.1126/science. 320. 5882. 1409

Su, P., Wang, X., Xie, T., Wang, X., Wang, L., Zhou, Z., & Shi, R. (2018). Inorganic carbon sequestration capacity and soil carbon assimilation pathway of deserts in arid region. *Chinese Science Bulletin*, *63*(8), 755–765. doi.org/10.1360/n972017-00891

Sun, Z.G., Wang, L.L., Tian, H.Q., Jiang, H.H., Mou, X.J., Sun, W.L. (2013) Fluxes of nitrous oxide and methane in different coastal Suaeda salsa marshes of the Yellow River estuary, China. *Chemospher*e, 90, 856 – 865.

Sutter, L. A., Perry, J. E., & Chambers, R. M. (2014). Tidal freshwater marsh plant responses to low level salinity increases. *Wetlands*, *34*(1), 167–175. doi.org/10.1007/s13157-013-0494-x

Szynkiewicz, A., Witcher, J. C., Modelska, M., Borrok, D. M., & Pratt, L. M. (2011). Anthropogenic sulfate loads in the Rio Grande, New Mexico (USA). *Chemical Geology*, *283*(3–4), 194–209. doi.org/10.1016/j.chemgeo.2011.01.017

Tang, H., Qiu, J., Van Ranst, E., & Li, C. (2006). Estimations of soil organic carbon storage in cropland of China based on DNDC model. *Geoderma*, *134*(1–2), 200–206. doi.org/10.1016/j.geoderma.2005.10.005

Tavakkoli, E., Fatehi, F., Coventry, S., Rengasamy, P., & McDonald, G. K. (2011). Additive effects of Na^+ and Cl^- ions on barley growth under salinity stress. *Journal of Experimental Botany*, *62*(6), 2189–2203. doi.org/10.1093/jxb/erq422

Tong, C., Huang, J. F., Hu, Z. Q., & Jin, Y. F. (2013). Diurnal variations of carbon dioxide, methane, and nitrous oxide vertical fluxes in a subtropical estuarine marsh on neap and spring tide days. *Estuaries and Coasts*, *36*(3), 633–642. doi.org/10.1007/s12237-013-9596-1

Tong, C., Wang, W. Q., Zeng, C. S., & Marrs, R. (2010). Methane (CH_4) emission from a tidal marsh in the Min River estuary, southeast China. *Journal of Environmental Science and Health - Part A Toxic/Hazardous Substances and Environmental Engineering*, *45*(4), 506–516. doi.org/10.1080/ 10934520903542261

van Dijk, G., Smolders, A. J. P., Loeb, R., Bout, A., Roelofs, J. G. M., & Lamers, L. P. M. (2015). Salinization of coastal freshwater wetlands; effects of constant versus fluctuating salinity on sediment biogeochemistry. *Biogeochemistry*, *126*(1–2), 71–84. doi.org/10.1007/s10533-015-0140-1

van Genuchten, M. T. (1980). Closed-form equation for predicting the hydraulic conductivity of unsaturated soils. *Soil Science Society of America Journal*, *44*(5), 892–898. doi.org/10.2136/sssaj1980.03615995004400050002x

Vizza, C., West, W. E., Jones, S. E., Hart, J. A., & Lamberti, G. A. (2017). Regulators of coastal wetland methane production and responses to simulated global change. *Biogeosciences*, *14*(2), 431–446. doi.org/10.5194/bg-14-431-2017

Wang, X. J., Xu, M. G., Wang, J. P., Zhang, W. J., Yang, X. Y., Huang, S. M., & Liu, H. (2014). Fertilization enhancing carbon sequestration as carbonate in arid cropland: assessments of long-term experiments in northern China. *Plant and Soil*, *380*(1), 89–100. doi.org/10.1007/s11104-014-2077-x

Wang, W.Q., Sardans, J., Wang, C., Zeng, C.S., Tong, C., Chen, G.X., Huang, J.F., Pan, H.R., Peguero, G.L., Vallicrosa, H.L.N., Peñuelas, J. (2019). The response of stocks of C, N and P to plant invasion in the coastal wetlands of China. Global Change Biology, 2019, 5(2): 733–743. doi.org/ 10.1111/gcb.14491

Weston, N. B., Giblin, A. E., Banta, G. T., Hopkinson, C. S., & Tucker, J. (2010). The effects of varying salinity on ammonium exchange in estuarine sediments of the Parker River, Massachusetts. *Estuaries and Coasts*, *33*(4), 985–1003. doi.org/10.1007/s12237-010-9282-5

Weston, N. B., Neubauer, S. C., Velinsky, D. J., & Vile, M. A. (2014). Net ecosystem carbon exchange and the greenhouse gas balance of tidal marshes along an estuarine salinity gradient. *Biogeochemistry*, *120*(1–3), 163–189. doi.org/10.1007/s10533-014-9989-7

Winter, T. C. (2000). The vulnerability of wetlands to climate change: a hydrologic landscape perspective. *Journal of the American Water Resources Association*, *36*(2), 305–311. doi.org/10.1111/j.1752-1688.2000.tb04269.x

Wu, X., Zhao, L., Fang, H., Zhao, Y., Smoak, J. M., Pang, Q., & Ding, Y. (2016). Environmental controls on soil organic carbon and nitrogen stocks in the high-altitude arid western Qinghai-Tibetan Plateau permafrost region. *Journal of Geophysical Research: Biogeosciences*, *121*(1), 176–187. doi.org/10.1002/ 2015JG003138

Xu, X., Zou, X., Cao, L., Zhamangulova, N., Zhao, Y., Tang, D., & Liu, D. (2014). Seasonal and spatial dynamics of greenhouse gas emissions under various vegetation covers in a coastal saline wetland in southeast China. *Ecological Engineering*, *73*, 469–477. doi.org/10.1016/j.ecoleng.2014.09.087

Ye, C., Zheng, M., Wang, Z., Hao, W., Wang, J., Lin, X., & Han, J. (2015). Hydrochemical characteristics and sources of brines in the Gasikule salt lake, Northwest Qaidam Basin, China. *Geochemical Journal*, *49*(5), 481–494. doi.org/10.2343/geochemj.2.0372

Zhang, Y., Wang, L., Xie, X., Huang, L., & Wu, Y. (2013). Effects of invasion of *Spartina alterniflora* and exogenous N deposition on N_2O emissions in a coastal salt marsh. *Ecological Engineering*, *58*, 77–83. doi.org/10.1016/ j.ecoleng. 2013.06.011

Zhou, J., Zhang, Y., Zhou, A., Liu, C., Cai, H., & Liu, Y. (2016). Application of hydrochemistry and stable isotopes ($\delta^{34}S$, $\delta^{18}O$ and $\delta^{37}Cl$) to trace natural and anthropogenic influences on the quality of groundwater in the piedmont region, Shijiazhuang, China. *Applied Geochemistry*, *71*, 63–72. doi.org/10.1016/ j.apgeochem.2016.05.018

Zou, J., Tobin, B., Luo, Y., & Osborne, B. (2018). Differential responses of soil CO_2 and N_2O fluxes to experimental warming. *Agricultural and Forest Meteorology*, *259*, 11–22. doi.org/10.1016/j.agrformet.2018.04.006

Figures

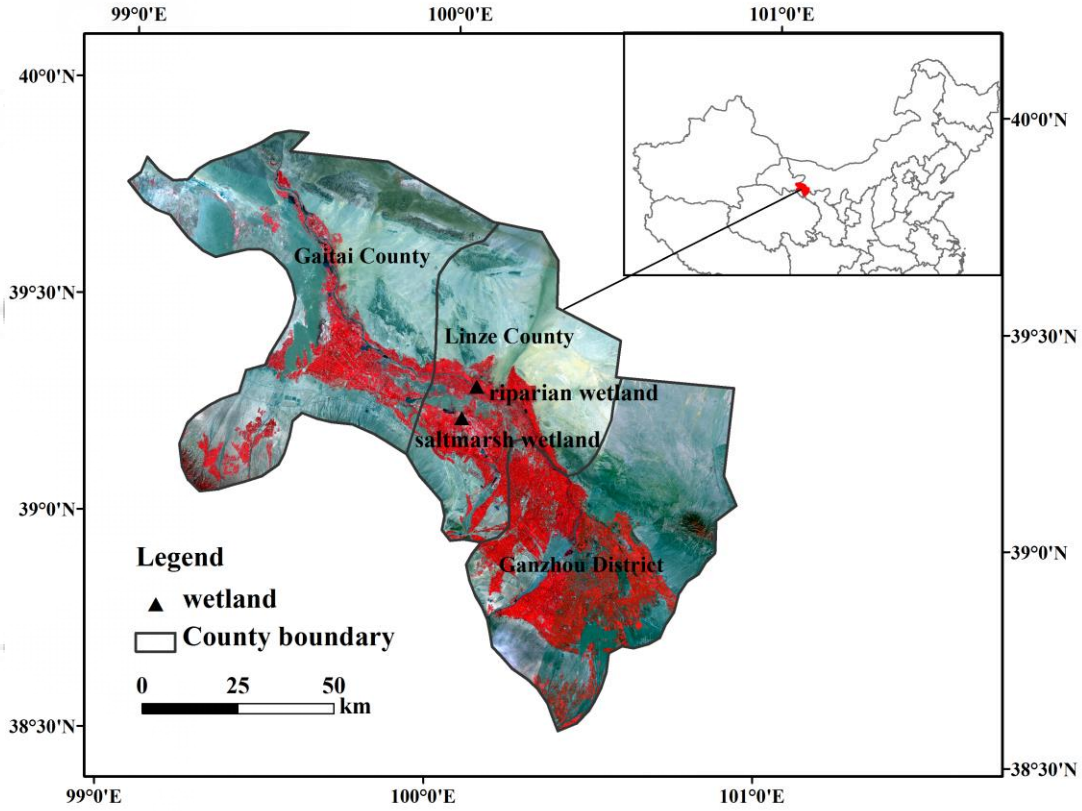

Fig. 1. Locations of the study area in China and of the riparian wetland and saltmarsh wetland within the study area.

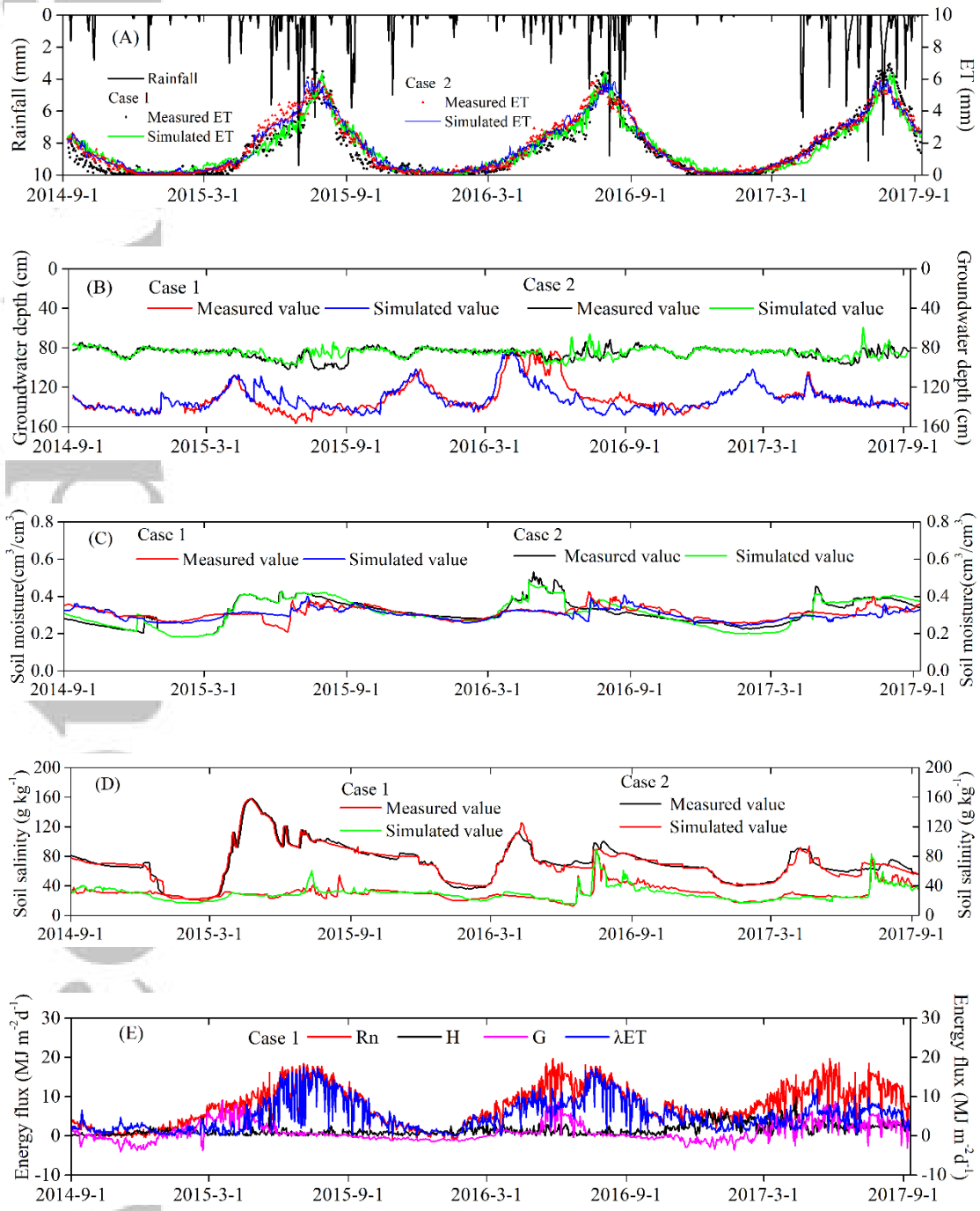

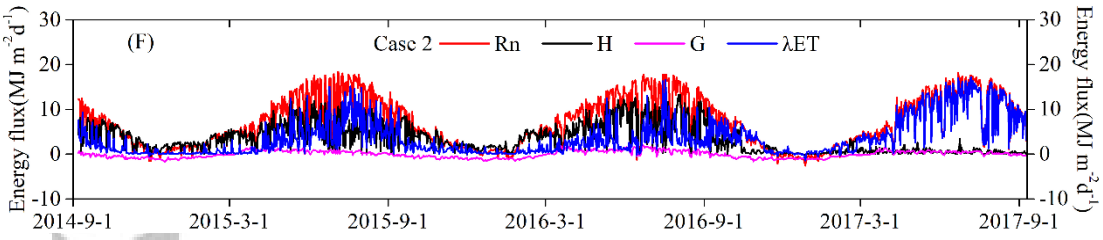

Fig. 2. The temporal variation of the measured and simulated values in the saltmarsh wetland (Case 1) and the riparian wetland (Case 2):(A) precipitation and evapotranspiration (*ET*); (B) groundwater depth; (C) soil moisture; (D) soil salinity; (E) energy flux terms (R_n, λ*ET*, *H* and *G*) in the riparian wetland; (F) energy flux terms (R_n, λ*ET*, *H* and *G*) in the saltmarsh wetland.R_n is the net radiation; *G* is the soil heat flux; *H* is the sensible heat flux; λ*ET* is the latent heat flux.

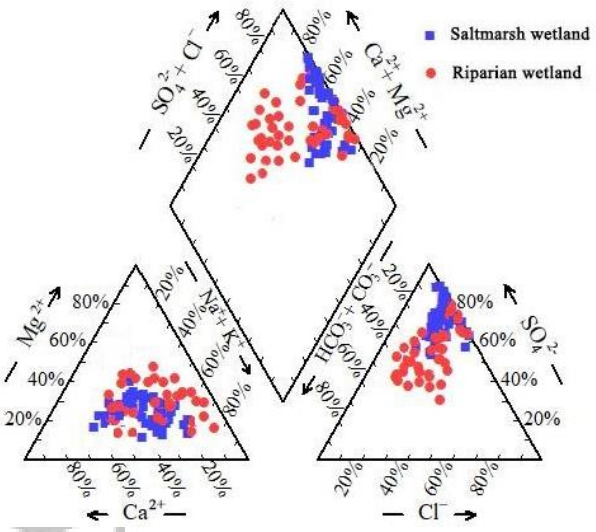

Fig. 3. Piper diagrams for cation and anion concentrations in the saltmarsh wetland and the riparian wetland.

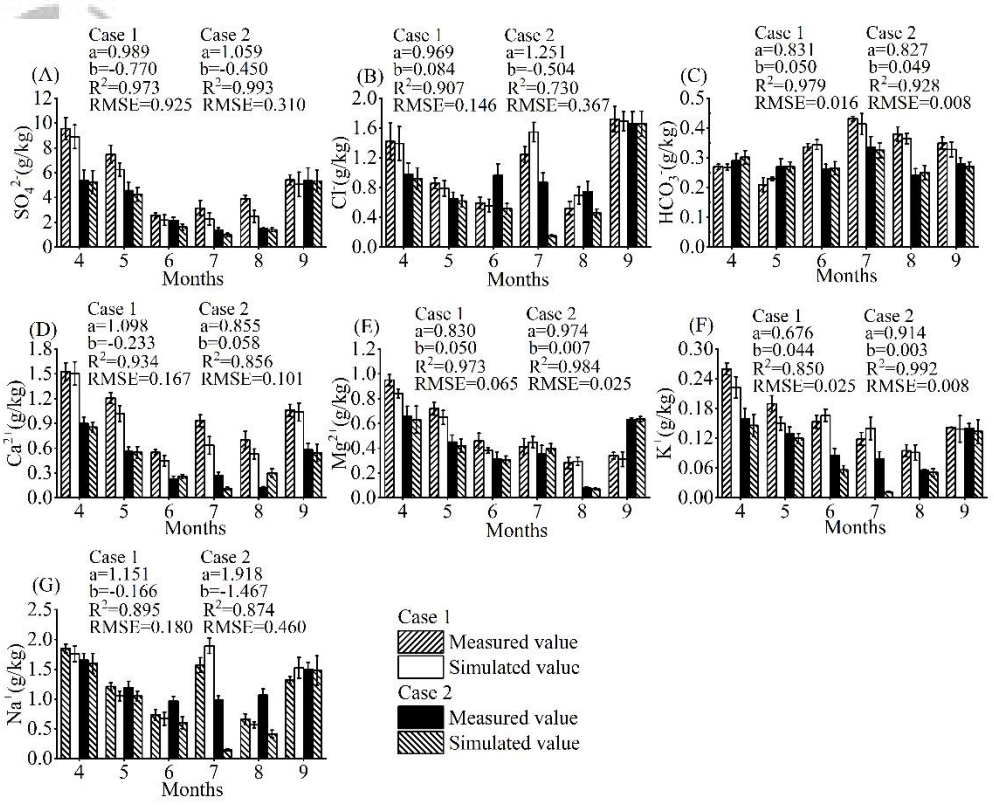

Fig. 4. The monthly variation of major ion concentrations during the growing season, and comparison of the measured and simulated values in the saltmarsh wetland (Case 1) and the riparian wetland (Case 2). Parameter definitions: *a* and *b* are regression coefficients for the equation $y = ax + b$ (where y = predicted and x is measured); R^2 is the goodness of fit for the regression, and RMSE is the root-mean-square error. All regressions were statistically significant ($P< 0.05$).

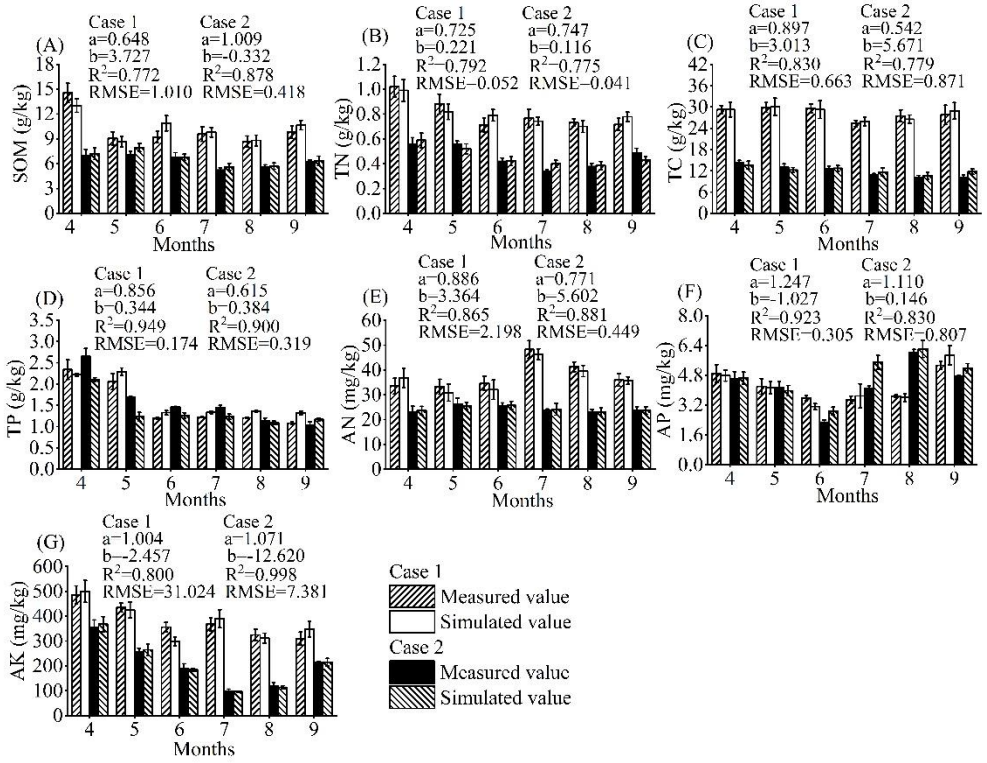

Fig. 5. The monthly variation of nutrient concentrations during the growing season, and comparison of the measured and simulated values, in the saltmarsh wetland (Case 1) and the riparian wetland (Case 2). Parameter definitions: *a* and *b* are regression coefficients for the equation $y = ax + b$ (where y = predicted and x is measured); R^2 is the goodness of fit for the regression, and RMSE is the root-mean-square error. All regressions were statistically significant ($P< 0.05$).

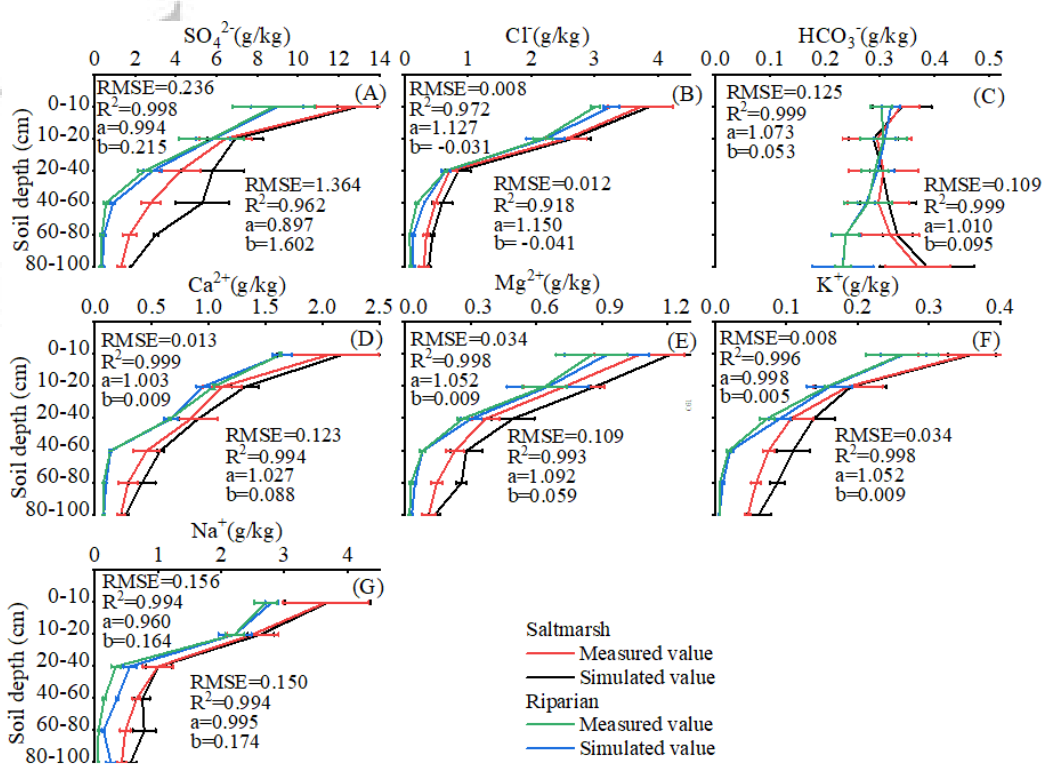

Fig. 6. Changes in major ion concentrations as a function of depth in the soil, and comparison between the measured and simulated values for the saltmarsh and the riparian wetland.

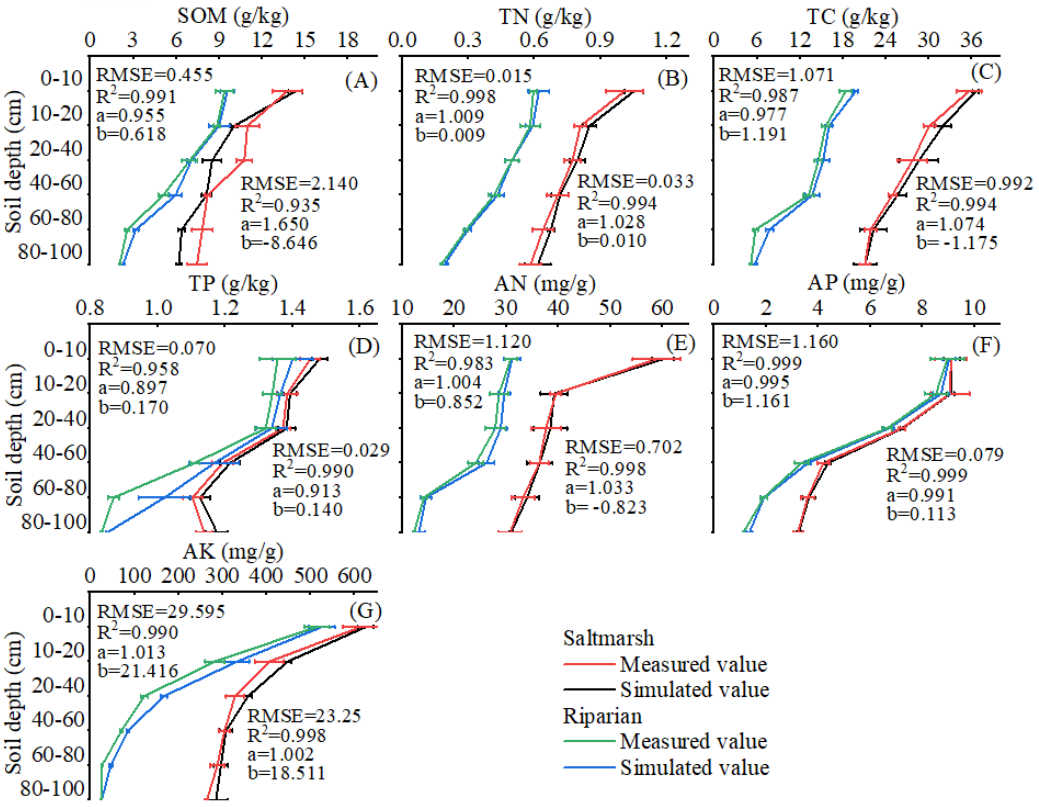

Fig. 7. Changes in the nutrient concentrations as a function of depth in the soil, and comparison between the measured and simulated values for the saltmarsh wetland and the riparian wetland.

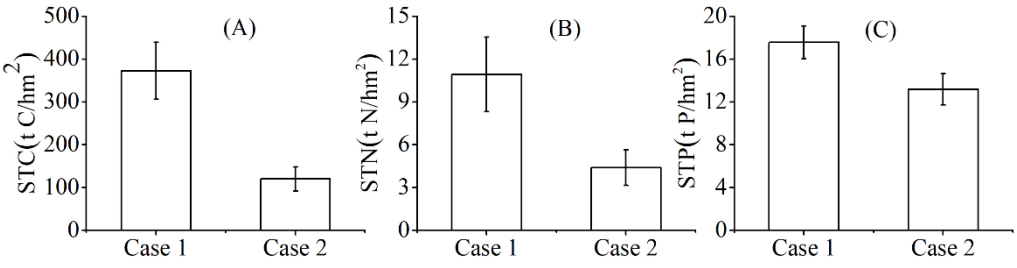

Fig. 8. The storage of total carbon (*STC*), total nitrogen (*STN*) and total phosphorus (*STP*) in the saltmarsh wetland (Case 1) and the riparian wetland (Case 2).

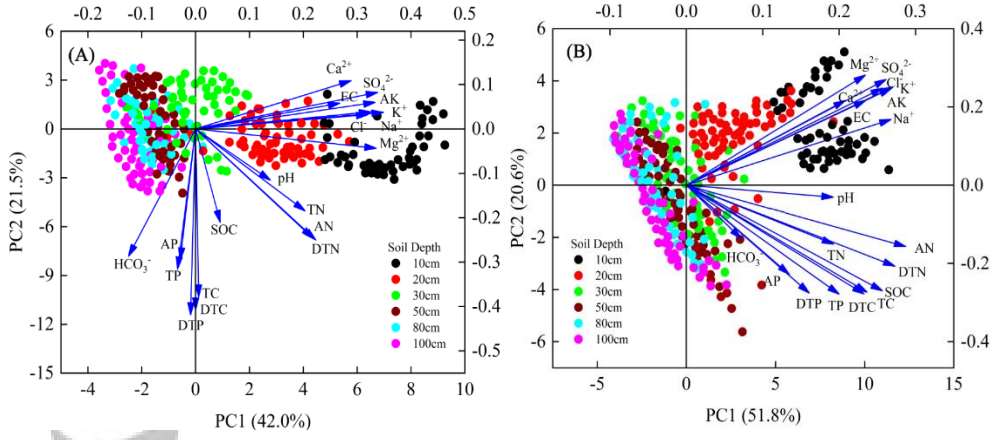

Fig. 9. The results of the canonical correlation analysis using the hydrochemical parameters for (A) the saltmarsh wetland and (B) the riparian wetland.

Table 1. Soil hydraulic parameters applied in the numerical simulation for each wetland

Wetland	Depth (cm)	θ_r ($cm^3\ cm^{-3}$)	θ_s ($cm^3\ cm^{-3}$)	α (cm^{-1})	n	K_s ($cm\ h^{-1}$)	l
Saltmarsh wetland	0-20	0.093	0.378	0.025	1.32	5.65	0.5
	20-40	0.071	0.495	0.022	1.56	1.52	0.5
	40-60	0.092	0.553	0.024	1.33	1.49	0.5
	60-80	0.131	0.538	0.034	1.08	1.20	0.5
	80-100	0.134	0.559	0.035	1.12	1.35	0.5
Riparian wetland	0-20	0.044	0.359	0.015	1.92	2.95	0.5
	20-40	0.014	0.441	0.008	2.32	4.33	0.5
	40-60	0.032	0.387	0.013	2.12	3.96	0.5
	60-80	0.025	0.377	0.012	2.27	4.15	0.5
	80-100	0.034	0.385	0.014	1.99	4.04	0.5

θ_r, θ_s, and K_s are the residual water content, saturated water content, and saturated hydraulic conductivity, respectively. α, n, and l are model parameters.

Table 4. Effects of wetland type (WT), soil depth (SD), sampling time (ST), and their interactions on hydrochemical characteristics in arid wetland. Abbreviations: VWC, volumetric water content; GW, depth to groundwater, TN, total nitrogen; TC, total carbon; TP, total phosphorus; AN, available nitrogen; AP, available phosphorus; AK, available potassium; TND, total nitrogen density; TCD, total carbon density; TPD, total phosphorus density.

	WT	SD	ST	WT × SD	WT × ST	SD × ST	WT × SD × ST
VWC (%)	3.56	2.64	82.35***	2.36	2.27	1.53	1.68
GW (cm)	1645***		1023***				
SOM	858.36***	175.71***	27.13***	53.32***	8.43***	32.07***	9.20***
TN	1329.10***	130.34***	24.97***	47.54***	18.49***	23.25***	7.71***
TC	2690.46***	25.82***	11.71***	149.08***	7.23***	11.94***	5.86***
TP	1.34	34.53***	12.76***	10.86***	9.06***	2.09**	2.29***
AN	1244.28***	101.94***	14.81***	61.83***	14.25***	22.80***	9.83***
AP	4.45*	234.32***	57.61***	155.16***	55.53***	69.97***	90.37***
AK	1663.52***	881.40***	224.20***	73.01***	55.69***	66.99***	45.54***
N:K	169499.62***	29089.72***	7349.46***	17735.43***	5262.61***	2657.94***	2369.68***
C:P	1880093.67***	40041.58***	31084.11***	107189.76***	4028.56***	12024.70***	6919.79***
C:K	1124795.71***	526033.71***	90761.92***	113887.85***	58236.69***	31136.58***	20114.05***
C:N	22757.76***	11245.74***	3258.86***	3470.02***	611.05***	1441.95***	682.29***
TND	14.88***	20.98***	22.03***	21.34***	63.25***	31.18***	91.26***
TCD	48.16***	18.23***	30.42***	32.48***	20.68***	21.17***	31.09***
TPD	32.99	67.93***	40.57***	70.86***	31.22***	60.71***	61.10***
HCO_3^-	627.31***	1766.14***	376.07***	36.68***	99.08***	96.25***	87.07***
SO_4^{2-}	52.68***	1636.95***	145.33***	41.83***	56.74***	86.59***	50.09***
Ca^{2+}	12.82***	17.39***	35.32***	75.03***	20.10***	12.52***	13.73***
Ca^{2+}	3510.78***	982.56***	158.50***	270.37***	210.03***	55.28***	51.72***
Mg^{2+}	133.30***	1751.92***	372.13***	45.11***	234.09***	124.02***	170.64***
K^+	603.53***	1759.79***	298.80***	26.90***	92.24***	78.28***	59.13***
Na^+	44.40***	1849.67***	223.86***	72.79***	107.76***	85.18***	80.98***

pH	1.34	0.91	1.90	0.48	0.29	0.76	0.57
EC	163.83***	713.40***	187.29***	45.38***	34.72***	121.41***	53.69***

Significance: ****P*< 0.001.

Table 5. The eigenvalues and intra-set correlations for the*TCD, TND,* and *TPD*in relation to the hydrochemical factors in the saltmarsh wetland and riparian wetland. Abbreviations: SOM, soil organic matter; TN, total nitrogen; TC, total carbon; TP, total phosphorus; AN, available nitrogen; AP, available phosphorus; AK, available potassium; *EC*, electrical conductivity.

	Saltmarshwetland					Riparian wetland				
	PC1	PC2	PC3	PC4	Total inertia	PC1	PC2	PC3	PC4	Total inertia
Eigenvalues	0.542	0.213	0.134	0.102	0.402	0.462	0.252	0.136	0.121	0.672
Correlation of *TCD*, *TND*, and *TPD* with the hydrochemical factors	0.760	0.256	0.179	0.125		0.814	0.383	0.231	0.138	
Cumulative percentage of variance explained										
For the hydrochemical factors	80.3	14.5	4.3	0.1		80.8	12.5	4.4	0.3	
For *TCD*, *TND*, and *TPD* – hydrochemical relationship	83.5	94.3	98.8	100.0		87.8	94.0	98.0	100.0	
Sum of all eigenvalues					0.991					0.971
Intra-set correlations										
SOM (g/kg)	0.046	-0.210	-0.246	0.471		0.257	-0.270	0.024	-0.009	

TN (g/kg)	0.203	-0.184	0.314	-0.168	0.193	-0.150	0.510	-0.160
TC (g/kg)	0.006	-0.379	-0.395	-0.257	0.236	-0.273	0.119	-0.005
TP (g/kg)	-0.033	-0.316	-0.009	0.387	0.200	-0.278	-0.392	0.173
AN (g/kg)	0.218	-0.246	0.375	-0.096	0.287	-0.157	0.143	-0.005
AP (mg/kg)	-0.028	-0.295	0.406	0.047	0.135	-0.228	-0.277	-0.360
AK (mg/kg)	0.333	0.060	-0.006	-0.060	0.268	0.248	-0.093	0.064
SO_4^{2-} (g/kg)	0.338	0.082	-0.077	-0.044	0.261	0.270	-0.037	-0.018
Cl^- (g/kg)	0.320	0.032	-0.139	0.165	0.257	0.248	-0.119	0.103
HCO_3^- (g/kg)	0.125	-0.287	0.173	0.329	0.072	-0.136	-0.497	-0.574
Ca^{2+} (g/kg)	0.389	0.109	-0.114	-0.129	0.208	0.217	-0.153	0.092
Mg^{2+} (g/kg)	0.335	-0.044	0.041	-0.011	0.234	0.281	-0.070	-0.020
K^+ (g/kg)	0.349	0.037	-0.044	0.003	0.270	0.251	0.010	-0.016
Na^+ (g/kg)	0.325	0.039	-0.118	0.151	0.268	0.168	0.089	-0.048

pH	0.139	-0.115	-0.329	0.429	0.192	-0.031	0.275	-0.457
EC	0.268	0.058	-0.114	0.134	0.235	0.216	-0.027	0.011